J Solid State Electrochem (1999) 3: 303–326

REVIEW

Vladislav V. Kharton · Aleksey A. Yaremchenko
Evgeny N. Naumovich

Research on the electrochemistry of oxygen ion conductors in the former Soviet Union. II. Perovskite-related oxides

Received: 5 November 1998 / Accepted: 26 November 1998

Abstract The review is devoted to the analysis of experimental results on electrochemical and physicochemical properties of the perovskite-related oxide phases obtained at scientific centers of the former Soviet Union. The main attention is focused on oxides with high electronic conductivity, which are potentially useful as electrodes for high-temperature electrochemical cells with oxygen-ion conducting solid electrolytes and interconnectors of solid oxide fuel cells, and on mixed ionic-electronic conductors for oxygen separation membranes. Along with perovskite-like solid solutions based on $LnMO_{3-\delta}$ (Ln is a rare-earth element, M = Cr, Mn, Fe, Co, Ni) and $SrCoO_{3-\delta}$, properties of the oxide phases $Ln_2MO_{4\pm\delta}$ (M = Cu, Ni, Co) with the K_2NiF_4-type structure are briefly reviewed.

Key words Perovskite · Conductivity · Oxygen permeability · Electrode · Thermal expansion

Introduction

Perovskite-related oxides are of great interest as materials for solid oxide fuel cells (SOFCs), oxygen separation membranes, membrane reactors for hydrocarbon partial oxidation, solid electrolyte oxygen pumps and sensors. Properties of such oxides, determined by cations occupying A and B sites of the ABO_3 perovskite crystal lattice as well as external conditions such as temperature and oxygen partial pressure, vary over a wide range and can be controlled by a partial substitution in both cation sublattices. In addition, there exist several derivative structures exhibiting unique transport properties (brownmillerite, orthoferrite, K_2NiF_4-type phases, Aurvillius and Ruddlesden-Popper series). This offers considerable scope for developing novel materials with predetermined characteristics required by specific applications.

The present part of our review, devoted to the developments of oxygen ion conductors in the former Soviet Union, is focused on the experimental results from studying perovskite-related oxide phases. Among the variety of such oxides, we have chosen only materials which are considered to be applicable in high-temperature electrochemical devices. This is, firstly, oxides with high electronic conductivity, promising for electrodes of solid-electrolyte cells and interconnectors of SOFCs. Secondly, our attention is given to the developments of mixed conductors for oxygen electrochemical membranes of various types. Since the number of recent publications concerning high-temperature superconductors and K_2NiF_4-type oxides is very large, we have made an attempt to briefly list the articles which may be interesting from the viewpoint of oxygen electrochemistry. Analogously, the research articles concerning perovskite-type proton conductors, the synthesis and processing of ceramics, and the thermodynamic properties of the oxides are only listed in order to provide corresponding references for scientists interested in such information. The authors did not take into consideration the mechanisms of electronic transport in perovskites and defect equilibria, more detailed analysis of which can be found in monographs [1, 2].

V.V. Kharton (✉) · A.A. Yaremchenko · E.N. Naumovich
Institute of Physicochemical Problems,
Belarus State University, 14 Leningradskaya Str.,
220080 Minsk, Republic of Belarus
e-mail: kharton@fhp.bsu.unibel.by
Tel.: +375-172-207681
Fax: +375-172-264696

Perovskite-type $LnCrO_3$ (Ln = La–Lu, Y)

Rare-earth element (REE) chromites with perovskite-like structure find wide applications as materials for interconnectors of SOFCs, heaters of high-temperature furnaces, and electrodes of various solid-electrolyte cells [1]. This is caused by such properties of the chromites as a high electronic conductivity at temperatures above

1170 K, high melting point, stability in both reducing and oxidative environments, as well as thermal expansion coefficients (TECs) close to that of stabilized zirconia.

Phase diagrams and selected phase relationships were reported for the Ln_2O_3–Cr_2O_3 systems with Ln = La [3–5], Nd [3, 5], Sm [3, 5, 11], Eu [5, 6, 11], Gd [3, 5, 7, 11], Pr and Tb [8], Dy [8, 9, 11], Y [3–5, 11], and Sc [3, 5, 10, 11]. Owing to the small ionic radii of Sc^{3+}, the perovskite phase in the system Sc_2O_3–Cr_2O_3 does not form [3, 5, 10]. Instead, there are relatively large fields of solid solutions based on chromia (up to 28 mol% Sc_2O_3) and scandia (up to 10 mol% Cr_2O_3) in this system. In the range of 73–85 mol% of Sc_2O_3, existing γ-solid solutions based on the the $Cr_2O_3{\cdot}3Sc_2O_3$ compound were reported [3, 5, 10, 11]. For other rare-earth elements (Ln = La–Lu, Y), except cerium, the formation of perovskite phases $LnCrO_3$ is observed [1, 3, 8]. Cerium chromite was found to be stable only in reducing atmospheres [8]. The phase diagrams of Ln_2O_3–Cr_2O_3 (Ln = La, Nd, Sm, Gd, Y) are similar to each other and characterized by extremely narrow fields of the forming solid solution [3, 11]. Perovskite-type chromites were ascertained to melt congruently in the temperature range of 2400–2800 K (Table 1), but the melting temperature tends to decrease with the decreasing ionic radii of the REE cations.

At high temperatures, REE chromites are subject to thermal dissociation associated with evaporating chromia [3]. Owing to the decreasing stability of the perovskites with a decreasing tolerance factor, the decreasing REE cation radii results in a decreasing degree of thermal dissociation. For example, the degree of decomposition of the $LaCrO_3$ and $YbCrO_3$ specimens after annealing in an argon atmosphere at 2100 K for 0.5 h was as high as 5–10 and 70 vol%, respectively [3]. The perovskite-type chromites were reported to be stable in relation to alkalis and numerous acids [8].

The crystal structure of $LnCrO_3$ corresponds to the orthorombically distorted perovskite at room temperature, transforming into the perovskite-like rhombohedral phase at 563 ± 5 K [3, 14]. The orthorhombic distortions increase regularly with the decreasing radii of the REE cations, and no "orthorhombic ↔ rhombohedral" phase transitions were established for chromites of Pr, Nd, Sm, and Y at temperatures below 1170 K [14]. The values of the thermal expansion coefficients (TECs) calculated from the dilatometric data are listed in Table 2.

Data on the kinetics of solid-state synthesis and sintering of $LnCrO_3$ as functions of temperature, starting materials, atmosphere, and preparation methods have been published [1, 8, 20–31]. In order to produce single-phase reactive powders of chromites, use of the techniques of either decomposition of metal nitrates (or organic precursors) or coprecipitation is desirable [1]. The solid state reactions in oxidative atmospheres were reported to be, as a rule, much faster in comparison with those in inert and reducing atmospheres. However, evaporation of chromia may occur in oxidizing atmospheres, resulting in formation of B-site-deficient perovskites and a variation in their properties [27]. In the reducing atmospheres, a partial incorporation of chromium cations into interstitials of the perovskite crystal lattice can take place [27]. The rate of the solid state synthesis can be increased by doping chromites with moderate amounts of copper oxide [22, 25] or lithium oxide [29, 30].

Table 1 High-temperature stability limits of perovskite phases

Ln	$LnCrO_3$				$LnCoO_3$			
	Process	Atmosphere	T (K)	Ref.	Process	Atmosphere	T (K)	Ref.
La	melting	argon	2790 ± 50	[8]				
	melting	argon	2703 ± 30	[4, 5]				
	melting	air	2703 ± 30	[4]				
Pr					melting	air	1793 ± 10	[12]
Nd	melting	argon	2690 ± 50	[8]	melting	air	1683 ± 10	[12]
	melting	argon	2603 ± 30	[5]				
Sm	melting	argon	2670 ± 50	[8]	melting	air	1617 ± 4	[13]
	melting	argon	2573 ± 30	[5]				
Eu	melting	argon	2550 ± 50	[8]	melting	air	1610 ± 4	[13]
	melting	argon	2573 ± 30	[5]				
	melting	argon	2563	[6]				
Gd	melting	argon	2618 ± 50	[8]	melting	air	1593 ± 10	[12]
	melting	argon	2623 ± 30	[5, 7]	decomposition	air	1528 ± 5	[13]
Tb	melting	argon	2560 ± 50	[8]	decomposition	air	1428 ± 5	[13]
Dy	melting	argon	2550 ± 50	[8]	decomposition	air	1358 ± 5	[13]
	melting	argon	2593 ± 30	[9]				
Ho	melting	argon	2528 ± 50	[8]	decomposition	air	1323 ± 5	[13]
Er	melting	argon	2470 ± 50	[8]				
Yb	melting	argon	2430 ± 50	[8]				
Lu	melting	argon	2530 ± 50	[8]				
Y	melting	argon	2583 ± 30	[4, 5]				
	melting	air	2583 ± 30	[4, 5]				

Table 2 Thermal expansion coefficients of $LnCrO_3$-based solid solutions calculated from dilatometric data

Composition	Averaged TEC values		Ref.
	Temperature range (K)	$\overline{\alpha} \times 10^6$ (K^{-1})	
$LaCrO_3$	300–500	7.5	[15]
	540–1020	9.5	
$La_{0.95}Ca_{0.05}CrO_3$	300–1270	8.35	[16]
$LaCr_{0.8}Co_{0.2}O_3$	570–970	14.6	[15]
$LaCr_{0.6}Co_{0.4}O_3$	570–970	18.7	[15]
$LaCr_{0.2}Co_{0.8}O_3$	570–970	20.9	[15]
$La_{0.7}Sr_{0.3}Cr_{0.2}Co_{0.8}O_3$	470–870	19.0	[17]
$La_{0.7}Sr_{0.3}Cr_{0.5}Co_{0.5}O_3$	470–870	19.0	[17]
$La_{0.7}Sr_{0.3}Cr_{0.8}Co_{0.2}O_3$	470–870	14.5	[17]
$PrCrO_3$	300–1180	8.5	[3]
$NdCrO_3$	300–1180	8.3	[3]
$Nd_{0.8}Ca_{0.2}Cr_{1-y}Ag_yO_3$ (y = 0–0.2)	600–1180	9.3–9.9	[18]
$Nd_{0.7}Ca_{0.3}Cr_{1-y}Ag_yO_3$ (y = 0–0.2)	600–1180	9.9–10.1	[18]
$Nd_{0.6}Ca_{0.4}Cr_{1-y}Ag_yO_3$ (y = 0–0.2)	600–1180	10.8–11.0	[18]
$Nd_{0.8}Ca_{0.2}Cr_{1-y}Zn_yO_3$ (y = 0–0.2)	600–1180	9.2	[19]
$Nd_{0.6}Ca_{0.4}Cr_{1-y}Zn_yO_3$ (y = 0–0.2)	600–1180	10.4	[19]
$SmCrO_3$	300–1180	8.6	[3]
$YCrO_3$	300–1180	7.9	[3]
$GdCrO_3$	300–1180	7.0	[3]

Among other important results, one can list the detailed X-ray diffraction (XRD) data [31, 32], the results on IR absorption [3], and thermodynamic properties of selected $LnCrO_3$ phases [33].

Electrical conduction in $LnCrO_3$ occurs by the small-polaron mechanism via transport of electron holes localized at chromium ions (Cr^{4+} cations) in the B sublattice [31, 34]. The oxygen ion transference numbers at a temperature of 1470 K were established to be less than 1×10^{-4} [31, 34]. The values of the Seebeck coefficient of $LnCrO_3$ are essentially independent of temperature in the range of 873–1273 K, which suggests a temperature independence of the charge carrier concentration. Zemtsov et al. [31, 34] reported an absence of monotonic dependence of electrical properties of the chromites on the lanthanide cationic radii. The minimum activation energy for electrical conductivity and maximum conductivity determined for samarium chromite was explained by the effect of the structure of the $4f$ shells of REE cations [31, 34]. Gordon et al. [35] found that the conductivity of $LnCrO_3$ (Ln = La, Nd, Sm, Y) at 1250–2300 K decreases in the sequence La > Nd > Y > Sm. Such dependence, correlating with the activation energy for conductivity [35], may be caused by an increasing overlap integral of the d-orbitals of chromium cations and the p-orbitals of oxygen anions with increasing lanthanide cation radii, which results in increasing mobility of electron holes [1, 2]. A decrease in oxygen partial pressure leads regularly to decreasing p-type conductivity [34]. The values of the conductivity for selected REE chromites and solid solutions based on them are presented in Tables 3 and 4.

The electrical conductivity of the chromites to a large extent depends on the preparation conditions and pre-history of the ceramics (Table 5). This is caused, firstly, by the possible incomplete solid state synthesis and a presence of impurity phases as well as by the additional sintering of the ceramics at high temperatures. In particular, annealing at temperatures above 1700 K was pointed out to result in increasing conductivity in cases where perovskite phase dissociation due to evaporation of chromia does not occur [27, 35, 45]. Secondly, the processes of oxygen exchange between chromites and the gas phase are relatively slow. As a result, the ceramics pre-annealed in atmospheres with a low oxygen pressure exhibit typically lower conductivity, compared to the specimens pre-annealed in air [27, 31, 35]. One should note also that the pre-history determines the amount of impurities affecting the conduction. For example, small impurities of copper and molybdenum oxides were demonstrated to increase conductivity of the lanthanum chromite ceramics [28].

The solid solutions $(Ln,A)CrO_{3-\delta}$ (A = Ca, Sr, Ba) and $Ln(Cr,Mg)O_{3-\delta}$

As introduction of divalent cations into the crystal lattice of REE chromites leads to a sharp increase of the conductivity, $LnCrO_3$ perovskites doped with alkaline earth elements (AEE) and magnesium have attracted considerable attention [31, 36, 41, 43–49]. In comparison with other alkaline-earth dopants, the largest concentration range of the existing single perovskite phase is characteristic of the $Ln_{1-x}Ca_xCrO_{3-\delta}$ ternary oxide systems. The range forming solid solutions in these systems was determined as $0 \le x \le 0.40$ for Ln = La [46, 47], Pr [31, 48], Nd [31, 41], Sm [31, 41], Eu [31, 43], Gd [31], and Y [46]. For Ln = Tb and Yb, the solid solution range is $0 \le x \le 0.20$ and $0 \le x \le 0.15$, respectively [48]. The maximum solid solubility of calcium in the A sublattice of the perovskites is a function of the synthesis

Table 3 Electrical conductivity of solid solutions on the basis of $LaCrO_3$

Composition	Conductivity (S/cm)		Activation energy		Ref.
	300 K	970 K	T (K)	E_A (kJ/mol)	
$LaCrO_3$	2.9×10^{-3}	0.34	300–1370	19.8	[36]
$La_{0.95}Ca_{0.05}CrO_3$	0.34	2.3	300–970	11.6	[37]
$La_{0.95}Ca_{0.05}Cr_{0.5}Co_{0.5}O_3$	0.40	63	370–570	19.3	[38]
$La_{0.95}Ca_{0.05}Cr_{0.8}Ni_{0.2}O_3$	0.14	–	300–970	19.0	[37]
$La_{0.8}Ca_{0.2}CrO_3$	0.44	7.1	300–1370	14.1	[36]
$La_{0.8}Ca_{0.2}Cr_{0.8}Fe_{0.2}O_3$	1.1×10^{-2}	9.2	–	–	[39]
$La_{0.8}Ca_{0.2}Cr_{0.5}Fe_{0.5}O_3$	2.0×10^{-2}	6.8	–	–	[39]
$La_{0.8}Ca_{0.2}Cr_{0.2}Fe_{0.8}O_3$	1.4×10^{-2}	12	–	–	[39]
$La_{0.8}Ca_{0.2}Cr_{0.8}Ni_{0.2}O_3$	0.10	18	300–970	22.1	[37]
$La_{0.85}Ca_{0.15}Cr_{0.8}Co_{0.2}O_3$	1.5	25	370–570	9.7	[38]
$La_{0.85}Ca_{0.15}Cr_{0.5}Co_{0.5}O_3$	1.1	1.3×10^{2}	370–570	19.3	[38]
$La_{0.85}Ca_{0.15}Cr_{0.2}Co_{0.8}O_3$	1.3	4.0×10^{2}	370–570	26.1	[38]
$La_{0.7}Ca_{0.3}CrO_3$	2.4	18	300–970	11.5	[37]
$La_{0.7}Ca_{0.3}Cr_{0.8}Co_{0.2}O_3$	3.3	45	370–570	9.7	[38]
$La_{0.7}Ca_{0.3}Cr_{0.5}Co_{0.5}O_3$	1.8	85	370–570	15.4	[38]
$La_{0.7}Ca_{0.3}Cr_{0.2}Co_{0.8}O_3$	11	1.8×10^{2}	370–570	14.5	[38]
$La_{0.5}Ca_{0.5}CrO_3$	7.1×10^{-2}	3.7	300–1370	18.4	[36]
$La_{0.7}Sr_{0.3}CrO_3$	1.4	15	–	–	[17]
$La_{0.7}Sr_{0.3}Cr_{0.5}Co_{0.5}O_3$	6.0	58	370–580	8.7	[17]
$La_{0.7}Sr_{0.3}Cr_{0.5}Co_{0.5}O_3$	3.0	1.9×10^{2}	370–580	16.4	[17]
$La_{0.7}Sr_{0.3}Cr_{0.2}Co_{0.8}O_3$	1.0×10^{2}	4.7×10^{2}	370–580	6.8	[17]
$La_{0.8}Sr_{0.2}Cr_{0.8}Ni_{0.2}O_3$	0.43	–	300–970	16.3	[37]
$LaCr_{0.8}Co_{0.2}O_3$	6.6×10^{-5}	–	–	–	[15]
$LaCr_{0.6}Co_{0.4}O_3$	1.0×10^{-3}	–	–	–	[15]
$LaCr_{0.4}Co_{0.6}O_3$	4.0×10^{-3}	–	–	–	[15]
$LaCr_{0.2}Co_{0.8}O_3$	3.2×10^{-2}	–	–	–	[15]
$LaCr_{0.8}Ni_{0.2}O_3$	0.14	8.2	300–970	18.1	[37]
$LaCr_{0.6}Ni_{0.4}O_3$	0.83	26	300–970	15.3	[37]
$LaCr_{0.4}Ni_{0.6}O_3$	24	82	300–970	8.5	[37]
$LaCr_{0.2}Ni_{0.8}O_3$	1.4×10^{2}	1.3×10^{2}	–	–	[37]

conditions and the purity of the starting materials, which leads to a definite variation in the literature data. For example, an oversimplified range forming the perovskite phase $Ln_{1-x}Ca_xCrO_{3-\delta}$ (Ln = La, Gd) has been published [36, 44].

Since the difference of the ionic radii of REE for strontium and barium cations is larger compared to calcium, the solid solution formation range for the systems $Ln_{1-x}A_xCrO_{3-\delta}$ (A = Sr, Ba) is narrower in relation to $Ln_{1-x}Ca_xCrO_{3-\delta}$. The $Ln_{1-x}Sr_xCrO_{3-\delta}$ solid solutions

Table 4 Electrical conductivity of REE chromites and solid solutions based on them

Composition	Conductivity (S/cm)		Activation energy		Ref.
	870 K	1270 K	T (K)	E_A (kJ/mol)	
$PrCrO_3$	8.0×10^{-2}	0.18	870–1270	28.0	[34]
$Pr_{0.8}Ca_{0.2}CrO_3$	7.1	9.9	870–1170	29.9	[40]
$Pr_{0.6}Ca_{0.4}CrO_3$	12	23	870–1170	26.1	[40]
$NdCrO_3$	0.13	0.17	870–1270	17.4	[34]
$Nd_{0.8}Ca_{0.2}CrO_3$	5.9	12	870–1170	27.0	[41]
$Nd_{0.6}Ca_{0.4}CrO_3$	13	24	870–1170	21.2	[41]
$Nd_{0.8}Ca_{0.2}Cr_{0.86}Ag_{0.14}O_3$	–	30	–	–	[18]
$Nd_{0.7}Ca_{0.3}Cr_{0.88}Ag_{0.12}O_3$	50	61	–	–	[18]
$Nd_{0.6}Ca_{0.4}Cr_{0.94}Ag_{0.06}O_3$	–	56	–	–	[18]
$Nd_{0.8}Ca_{0.2}Cr_{0.88}Zn_{0.12}O_3$	–	40	–	–	[19]
$Nd_{0.7}Ca_{0.3}Cr_{0.92}Zn_{0.08}O_3$	46	52	–	–	[19]
$Nd_{0.6}Ca_{0.4}Cr_{0.94}Zn_{0.06}O_3$	–	80	–	–	[19]
$SmCrO_3$	0.32	0.39	870–1270	14.5	[34]
$SmCr_{0.5}Co_{0.5}O_3$	1.0×10^{-2}	–	–	–	[42]
$SmCr_{0.5}Ni_{0.5}O_3$	4.3	–	–	–	[42]
$EuCrO_3$	8.7×10^{-2}	0.11	870–1270	16.4	[34]
$Eu_{0.8}Ca_{0.2}CrO_3$	3.9	9.7	870–1270	32.8	[43]
$Eu_{0.6}Ca_{0.4}CrO_3$	8.0	14	870–1270	23.2	[43]
$GdCrO_3$	4.5×10^{-2}	7.6×10^{-2}	300–1370	18.7	[44]
$Gd_{0.8}Ca_{0.2}CrO_3$	3.8	4.7	300–1370	13.6	[44]
$Gd_{0.5}Ca_{0.5}CrO_3$	3.8	4.7	300–1370	13.1	[44]

Table 5 Electrical conductivity of $LaCrO_3$ as a function of preparation and measurement conditions

Conditions of preparation	Relative density (%)	Conditions of measurement	Conductivity (S/cm)		Ref.
			1270 K	2000 K	
Solid state synthesis by standard ceramic technology using oxides as starting materials. Sintering in air at 1700 K for 4 h	–	in air	0.17	–	[34]
Solid state synthesis by standard ceramic technology using oxides as starting materials (1500–1550 K is air for 25–30 h). Sintering in air at 1900 K for 3–6 h	71	in air	0.42	–	[36]
Synthesis by decomposing nitrates with subsequent annealing in air at 1270 K for 5–10 h. Sintering in argon atmosphere at 2170 K	71	in vacuum (10^{-2}–10^{-3} Torr)	0.18	0.76	[35]
Plasma synthesis with subsequent sintering in argon atmosphere at 2200 K and annealing in helium atmosphere at 1800 K for 8–10 h	~90	in helium (p_{O_2} = 0.1 Pa)	0.18	0.87	[27]
Plasma synthesis with subsequent sintering in argon atmosphere at 2200 K and annealing in argon atmosphere at 1800 K for 8–10 h	~90	in argon (p_{O_2} = 10 Pa)	3.7×10^{-2}	–	[27]
Plasma synthesis with subsequent sintering in argon atmosphere at 2200 K and annealing in air at 1350 K for 8–10 h	~90	in air	1.8×10^{-2}	0.87	[27]
Plasma synthesis with subsequent sintering in argon atmosphere at 2200 K and annealing in air at 1550 K for 8–10 h	~90	in air	5.6×10^{-2}	0.87	[27]
Plasma synthesis with subsequent sintering in argon atmosphere at 2200 K and annealing in air at 1800 K for 8–10 h	~90	in air	0.37	0.87	[27]

were ascertained to form at $0 \le x \le 0.30$ for Ln = La [47], $0 \le x \le 0.15$ for Pr and Eu [48], $0 \le x \le 0.05$ for Tb [48], and $0 \le x \le 0.05$ for Y [46]. For $Ln_{1-x}Ba_xCrO_{3-\delta}$, the single perovskite phase exists in the range $0 \le x \le 0.10$ for Ln = La and Pr [46, 48], and $0 \le x \le 0.05$ for Eu, Gd, Tb, and Y [46, 48].

The small radii of magnesium cations allows their incorporation only into the chromium sublattice, which is confirmed by published results [46]. The concentration limits for forming the solid solutions $LnCr_{1-x}Mg_xO_{3-\delta}$ (Ln = La–Gd) is from $x = 0.15$ to 0.40, depending on the lanthanide cation size and the synthesis conditions [1].

Introducing strontium and barium into the chromite crystal lattice leads to an increasing unit cell volume and a decreasing distortion of the perovskite structure [48]. The effect of doping by calcium depends on the relationship between the radii of the calcium and lanthanide cations, whereas substituting chromium with magnesium results in a decreasing unit cell volume [1, 31, 48]. The "orthorhombic ↔ rhombohedral" phase transition temperature of lanthanum chromite decreases with doping by strontium and increases when lanthanum is substituted by calcium [47].

The electrical conductivity of the solid solutions increases with the divalent dopant content within the single phase formation limits, caused by an increasing concentration of electron holes (Cr^{4+} ions) [31, 36, 37, 40, 41, 43, 44, 47, 49]. For the substituted chromites, the conductivity was established not to depend on the lanthanide cation radii, being a function only of dopant concentration [45]. Separation of the phase impurities results in decreasing conductivity. The electronic conduction decreases also with reducing oxygen partial pressure owing to removal of oxygen from the crystal lattice and a decreasing Cr^{4+} concentration.

Perovskite-type solid solutions $(Ln,A)(Cr,M)O_{3-\delta}$ (M = Al, Fe, Co, Ni, Cu, Zn, Ag)

Simultaneous doping into both A and B sublattices permits variation of the properties of the chromites over wide limits [1]. As a rule, properties of $Ln(Cr,M)O_{3-\delta}$ are intermediate between those of the basic perovskites $LnCrO_3$ and $LnMO_3$, while the solid solubility of M cations forming no perovskite phase with REE oxides is extremely limited.

In the $GdCrO_3$–$GdAlO_3$ pseudobinary system, the formation of a continuous series of solid solutions with an orthorombically distorted perovskite structure has been described [50]. The perovskite phase of $YbCr_{1-x}Al_xO_3$ exists only at $0 \le x \le 0.35$ [50].

The unlimited solubility of iron and cobalt cations in the B sublattice is typical for lanthanum chromite: the solid solutions of $La_{1-y}A_yCr_{1-x}M_xO_{3-\delta}$ (M = Fe or Co; A = Ca or Sr; $y = 0$–0.3) form in all concentration ranges for $0 \le x \le 1.0$ [15, 17, 38, 39, 47, 51]. The "orthorhombic ↔ rhombohedral" phase transition temperature decreases with cobalt additions [47]. The electronic conduction in such oxides was reported to occur mainly via hole transport between ions of cobalt and iron. As a result, the electrical conductivity of the perovskites

increases with increasing x and y [15, 17, 38, 39]. Substituting chromium with cobalt leads to increased thermal expansion, whereas doping with iron decreases the TECs (Table 2). The stability of the perovskite phases at low oxygen pressures increases with the chromium content [17]. In contrast to the stability, both oxygen permeability and ionic conductivity of the $La(Cr,Co)O_{3-\delta}$ solid solutions were shown to decrease regularly when the chromium concentration increased [52].

Since the stability of perovskite-like nickelates $LnNiO_{3-\delta}$ is considerably less compared to the ferrites and cobaltites, the solid solutions of $LnCr_{1-x}Ni_xO_{3-\delta}$ exist only within limited concentration ranges at a high chromium content [1]. This range depends on the preparation conditions and becomes narrower with decreasing lanthanide cation radii. The perovskite $LaNiO_{3-\delta}$ is known to be stable in air at temperatures below 1170 K; increasing the oxygen pressure leads to increasing stability of this phase (see section on $LnNiO_{3-\delta}$ below). Therefore the concentration range of existing $LnCr_{1-x}Ni_xO_{3-\delta}$ solid solutions expands with decreasing synthesis temperature and with increasing partial pressure of oxygen. In particular, this range for Ln = La at temperatures above 1300 K in air corresponds to $0 \le x \le 0.6$, and the phases of $La_4Ni_3O_{10}$ and NiO were observed to separate at higher nickel content [37, 47]. For the oxides prepared by hydroxide coprecipitation and then annealed at 1170 K, the single perovskite phase forms at $0 \le x \le 1.0$ (Ln = La) and $0 \le x \le 0.4$ (Ln = Sm) [53]. The perovskites $LnCr_{1-x}Ni_xO_{3-\delta}$ (Ln = Gd and Yb), prepared by the coprecipitation of carbonates, are single phase at $0 \le x \le 0.15$ [54]. Introducing nickel into the chromium sublattice results in a drastic increase of electronic transport (Table 3) and in a transition to metallic conductivity typical for $LaNiO_{3-\delta}$ [37]. Here, the substitution of lanthanum with Ca or Sr causes narrowing of the solid solution formation range owing to increasing oxygen nonstoichiometry. No significant changes in the conductivity were observed when $LaCr_{1-x}Ni_xO_{3-\delta}$ were doped by the alkaline earth cations [37].

In the binary oxide systems Ln_2O_3–CuO and Ln_2O_3–ZnO there exist no perovskite phases in air [55–57]. The solid solubility of copper and zinc in the B sublattice of the perovskite-type chromites is relatively low. The perovskites phases of $LnCr_{1-x}Cu_xO_{3-\delta}$ (Ln = La, Gd, Yb) were found to form at $0 \le x \le 0.10$ [54]. For $LnCr_{1-x}Zn_xO_{3-\delta}$, formation of perovskites takes place at $0 \le x \le 0.15$ for Ln = La [54], $0 \le x \le 0.20$ for Nd [19], and $0 \le x \le 0.10$ for Gd and Yb [54]. Annealing $LnCr_{1-x}Zn_xO_{3-\delta}$ (Ln = La, Gd, Yb) prepared by carbonate coprecipitation leads to a partial decomposition of the solid solutions at 1470 K in air, and the perovskite phases form only in the range $0 \le x \le 0.10$ [54]. Similar to doping by alkaline earth elements, addition of moderate amounts of zinc (up to 10–12 mol%) provides an increase in the conductivity of the chromites [19]. The oxygen ion transference numbers of the $Nd_{0.8}Ca_{0.2}Cr_{0.88}Zn_{0.12}O_{3-\delta}$ ceramics were determined by Faradaic efficiency measurements at 1140 K to be 2.7×10^{-6}, which corresponds to a value for the ionic conductivity of 9.4×10^{-5} S/cm [19].

Formation of $Nd_{1-x}Ca_xCr_{1-y}Ag_yO_{3-\delta}$ ($0.2 \le x \le 0.4$, $0 \le y \le 0.10$) solid solutions has also been reported [18]. The properties of these oxides are close to that of neodymium chromite doped with calcium and zinc [19]. Introducing silver into the chromium sublattice at $y = 0.12$–0.16 increases the conductivity [18]. The electrical conductivity of $Nd_{1-x}Ca_xCr_{1-y}M_yO_{3-\delta}$ (M = Zn, Ag) depends very weakly on the oxygen pressure in the range $10^{-5} \le p_{O_2} \le 10^5$ Pa and decreases with further decreasing oxygen content in the gas phase [18, 19].

Perovskite-like manganites $LnMnO_{3\pm\delta}$ and $(Ln,A)MnO_{3\pm\delta}$ (A = Ca, Sr, Ba, Pb, Cd)

Perovskite-type manganites of rare-earth elements possess considerably higher conductivity and electrochemical activity compared to the chromites, whereas the TECs of manganites are close to the TECs of stabilized zirconia ceramics [1]. Owing to this, manganites are considered to be the most promising materials for oxygen electrodes of SOFCs and other electrochemical cells with ZrO_2-based electrolytes. Despite the high conductivity, manganite ceramics cannot be used as interconnectors owing to the higher oxygen permeability and worse stability in reducing atmospheres in comparison with the REE chromites.

Data on selected phase relationships and crystal structures of some oxide phases in the systems Ln_2O_3–MnO_x have been published [58–62]. Formation of perovskite-like phases of $LnMnO_{3\pm\delta}$ was established for all the binary systems with REE and manganese oxides, except cerium. When annealing the CeO_2–MnO_x mixtures, only two-phase mixtures of ceria and manganese oxides were obtained [59]. For the systems with Ln = Nd-Lu and Y, there exist also $LnMn_2O_5$ phases in air at relatively low temperatures [59]. For Ln = Nd, Sm, Eu, Gd, Tb, Dy, or Ho, the $LnMn_2O_5$ compounds are stable up to 1370 K [59]. In the case of Ln = Er, Yb, Lu, and Y, these oxides were reported to be stable only below 1270 K and to largely decompose after annealing at 1370 K, forming $LnMnO_3$ and Mn_3O_4 [59]. Only the perovskite-type phase with the oxygen nonstoichiometry varying over a large range can be obtained in air and in vacuum for the system La_2O_3–MnO_x [60, 61].

The crystal structure of the perovskite-like phases $LnMnO_3$ depends to a large degree on the preparation conditions, which determine the defect concentrations in the cation and anion sublattices [58]. For instance, data have been published on the formation in air of the perovskite phase of $LaMnO_{3\pm\delta}$ with rhombohedral [58, 63, 64], orthorhombic [60, 61] and monoclinic [60] distortions. A definite oxygen hyperstoichiometry ($\delta = 0.02$–0.05) is characteristic of lanthanum manganite

synthesized in air at 1000–1570 K, while the stoichiometric oxide can be obtained by annealing at 1670 K in air [60]. The structure of neodymium and gadolinium manganites was ascertained to be the orthorombically distorted perovskite [58, 65, 66]. When synthesized in air by the standard ceramic route or by the decomposition of metal nitrates, manganites of yttrium and ytterbium possess the ilmenite-type hexagonal structure [58, 67], but using the hydroxide coprecipitation technique allows preparation of $YMnO_{3+\delta}$ with the perovskite lattice [62]. Oxygen hyperstoichiometry of the manganites at room temperature in air tends to decrease with the decreasing radii of the REE cations [58]. At low oxygen partial pressures, $LaMnO_{3\pm\delta}$ decomposes to lanthanum oxide and MnO without intermediate formation of a phase with the K_2NiF_4-type structure [61]. Electronic conduction in $LnMnO_{3\pm\delta}$ was reported to occur via hopping electron holes between manganese cations and to decrease with decreasing lanthanide cation radii [58]. The conductivity of $LnMnO_{3\pm\delta}$ with Ln = Nd, Gd, Y, or Yb in air was demonstrated by the Seebeck coefficient measurements to be p-type [58]. For $LaMnO_{3\pm\delta}$, heating in air results in a conversion of p-type to n-type conductivity at temperatures of 500–650 K, depending on the pre-history of the specimens.

Doping $LnMnO_3$ by divalent metal cations (Ca, Sr, Ba, Pb) leads to increasing Mn^{4+} ion concentration, which determines both the electrical and magnetic properties of the manganites and influences their crystal lattice [63–74]. The maximum values of x, corresponding to the upper limit of forming solid solutions of $Ln_{1-x}A_xMnO_{3-\delta}$ (Ln = La, Nd, Gd; A = Ca, Sr, Ba, Pb), were reported to vary from 0.4 to 0.6 [58, 65, 69, 70, 72]. In the system $La_{1-x}Cd_xMnO_{3-\delta}$ the solid solutions exist at $x = 0$–0.3 [72]. As a rule, the distortions of the perovskite-type structure decreases when the divalent cations are incorporated into the A sublattice. For $Ln_{1-x}Ca_xMnO_{3-\delta}$ (Ln = Y, Yb) at $0 < x \leq 0.4$, two coexisting phases with hexagonal ilmenite-type and orthorhombic perovskite-type structures were found [58, 67]. Further increases in calcium concentration result in the formation of the single perovskite phase [58, 67].

Electrical conductivity and Seebeck coefficients of the $Ln_{1-x}A_xMnO_{3-\delta}$ solid solutions at moderate divalent dopant contents were ascertained to increase with x, correlating well with the Mn^{4+} ion concentration [63–67, 69]. The maximum electrical conductivity corresponds to the values of $x = 0.2$–0.5, whereas shift of the conductivity maximum to that at a lower dopant concentration is typically observed with increasing temperature. Further increases in x lead to a decrease in conductivity, which is associated with decreasing mobility of the electronic charge carriers and is accompanied with a transition from p-type to n-type conductivity [58]. In some cases, such a decrease in conductivity is accompanied by the appearance of phase impurities in the manganite ceramics [63, 70]. Selected data on the conductivity of REE manganites and solid solutions based on them are shown in Table 6.

Thermal expansion coefficients of the manganite ceramics were calculated from the dilatometric data to decrease with decreasing REE cation radii and to increase with increasing concentrations of either calcium or strontium [58, 63–67, 81]. For the solid solutions with the maximum conductivity, the TECs are sufficiently close to those of stabilized zirconia electrolytes (Table 7).

One should note that both the electrical conductivity and thermal expansion of manganites are functions of the pre-history of the ceramics [1, 58]. This is determined primarily by the effect of the pre-history on the defect concentrations in cation and anion sublattices. For example, quenching $La_{1-x}Ca_xMnO_{3-\delta}$ ceramics after annealing in air at 1720 K usually leads to a decrease in conductivity and an increase in activation energy for electrical conductivity compared to the specimens cooled slowly [58, 63]. The highest values of the conductivity were obtained for the manganite ceramics prepared by the methods of hydroxide coprecipitation and thermal decomposition of metal nitrates [62].

Doping lanthanum manganite with calcium was demonstrated to increase the sinterability of the ceramics [70]. The sinterability and electrical conductivity can be also achieved by adding small amounts of CuO or Bi_2CuO_4 to the manganite ceramics [81, 83–86]. Sintering aids such as bismuth oxide and Bi_2CuO_4 provide improved electrochemical properties of the manganite electrode layers, which will be considered in the final section below on electrode properties.

The oxygen permeability of dense ceramic membranes of lanthanum-strontium manganites has been studied [69, 81, 84–89]. Oxygen permeation fluxes obtainable using manganite membranes were stated to be considerably less in comparison with lanthanum-strontium cobaltite membranes [87, 88]. The permeation fluxes through manganite ceramics are limited by the interphase oxygen exchange rate at the membrane/gas boundaries and can be enhanced by applying layers of dispersed platinum, praseodymium oxide, or their mixtures onto the membrane surfaces [81, 89]. Creation of cation vacancies in the A sublattice of lanthanum-strontium manganites may result in increasing oxygen permeability [81]. The permeability of $(La,Pb)MnO_{3-\delta}$ solid solutions is noticeably less compared to that of $(La,Sr)MnO_{3-\delta}$ at the same dopant concentrations [69, 81], which may be due to either a partial evaporation of lead oxide during the solid state synthesis or to specific electronic properties of lead cations [90].

The solid solutions $(Ln,Sr)(Mn,M)O_{3-\delta}$ (M = Ti, Fe, Co, Ni)

Partial substitution of manganese with other transition metals leads to substantial variations in conductivity, in oxygen permeability of manganite ceramic membranes, and in the electrochemical activity of manganite electrodes [1, 75, 76, 81].

Table 6 Electrical conductivity of solid solutions based on $LnMnO_3$

Composition	Conductivity (S/cm)		Activation energy		Ref.
	300 K	1000 K	T (K)	E_A (kJ/mol)	
$LaMnO_3$	4.4	81	300–580	11.0	[64]
$La_{0.8}Ca_{0.2}MnO_3$	6.7	1.5×10^2	320–520	6.3	[63]
			550–1050	10.6	
$La_{0.6}Ca_{0.4}MnO_3$	5.6	74	350–1050	9.3	[63]
$La_{0.5}Ca_{0.5}MnO_3$	1.4	1.3×10^2	350–1050	10.7	[63]
$La_{0.8}Sr_{0.2}MnO_3$	43	1.6×10^2	300–1100	5.5	[64]
$La_{0.6}Sr_{0.4}MnO_3$	1.2×10^2	2.0×10^2	410–835	4.9	[64]
$La_{0.5}Sr_{0.5}MnO_3$	1.1×10^2	1.4×10^2	300–650	2.1	[64]
$La_{0.6}Sr_{0.4}Mn_{0.8}Fe_{0.2}O_3$		49			[75]
$La_{0.6}Sr_{0.4}Mn_{0.6}Fe_{0.4}O_3$		4.7			[75]
$La_{0.6}Sr_{0.4}Mn_{0.5}Fe_{0.5}O_3$		8.6			[75]
$La_{0.6}Sr_{0.4}Mn_{0.8}Ni_{0.2}O_3$		1.6×10^2			[76]
$La_{0.6}Sr_{0.4}Mn_{0.6}Ni_{0.4}O_3$		2.8×10^2			[76]
$La_{0.8}Pb_{0.2}MnO_3$		1.5×10^2			[69]
$La_{0.6}Pb_{0.4}MnO_3$		2.0×10^2			[69]
$La_{0.5}Pb_{0.5}MnO_3$		2.0×10^2			[69]
$LaMn_{0.8}Ti_{0.2}O_3$	5.6×10^{-2}	10	300–1000	17.5	[77]
$CaMnO_3$	1.0	7.9	300–700	5.9	[78]
$CaMn_{0.8}Ti_{0.2}O_3$	2.4×10^{-2}	5.0	300–700	23.3	[78]
$NdMnO_3$	4.3×10^{-2}	76	300–1070	26.2	[66]
$Nd_{0.8}Ca_{0.2}MnO_3$	1.0	1.6×10^2	300–1070	23.0	[66]
$Nd_{0.6}Ca_{0.4}MnO_3$	6.2×10^{-2}	10	300–1070	20.1	[66]
$Nd_{0.5}Ca_{0.5}MnO_3$	1.2×10^{-3}	2.0	300–1070	29.2	[66]
$GdMnO_3$	3.0×10^{-3}	2.8	300–1070	26.7	[65]
$Gd_{0.8}Ca_{0.2}MnO_3$	0.30	26	300–1070	18.8	[65]
$Gd_{0.6}Ca_{0.4}MnO_3$	0.89	1.8×10^2	300–1070	19.4	[65]
$Gd_{0.5}Ca_{0.5}MnO_3$	0.16	1.5×10^2	300–1070	27.6	[65]
$YbMnO_3$	7.2×10^{-6}	7.5×10^{-3}	300–1100	94.2	[67]
$Yb_{0.6}Ca_{0.4}MnO_3$	1.8	1.3×10^2	300–1100	18.8	[67]
$Yb_{0.5}Ca_{0.5}MnO_3$	4.1	1.8×10^2	300–1100	14.4	[67]
$YMnO_3$	6.8×10^{-6}		300–1100	98.1	[79]
$Y_{0.6}Ca_{0.4}MnO_3$	1.1		300–650	20.1	[79]
			650–1100	18.4	
$Y_{0.5}Ca_{0.5}MnO_3$	1.6		300–1100	16.8	[79]
$Bi_{0.6}Sr_{0.4}MnO_3$	0.28	20			[80]
$Bi_{0.5}Sr_{0.5}MnO_3$	0.5	45			[80]

The pseudobinary oxide system $LaMnO_3$–$La_2Ti_2O_7$ was studied by Korolev and Kononyuk [77]. The perovskite-type solid solutions $LaMn_{1-x}Ti_xO_{3\pm\delta}$ were reported to form in the range $0 \le x \le 0.2$, whereas solid solutions with the pyrochlore structure exist at $0.9 \le x \le 1.0$ [77]. For the perovskite phase, incorporation of titanium into the manganese sublattice results in an increase in the Seebeck coefficient and a decrease in the conductivity (Table 6). The TECs of the $LaMn_{1-x}Ti_xO_{3\pm\delta}$ ceramics were ascertained to slightly decrease with x [77]. In particular, the TEC value of the $La_2Ti_{1.8}Mn_{0.2}O_{7-\delta}$ pyrochlore in the temperature range 320–1000 K is $9.4 \times 10^{-6}\,K^{-1}$.

The electrical conductivity of the $La_{0.6}Sr_{0.4}Mn_{1-x}Fe_xO_{3-\delta}$ ($x = 0$–0.5) solid solutions decreases with iron additions, while the rhombohedrally distorted perovskite unit cell volume increases [75]. In the $LaMn_{1-x}Ni_xO_{3-\delta}$ system, perovskite-like solid solutions were found to exist at $0 \le x \le 0.5$ [91]. As doping with strontium decreases the thermodynamic stability of manganites, the single perovskite phase of $La_{0.6}Sr_{0.4}Mn_{1-x}Ni_xO_{3-\delta}$ with a rhombohedrally distorted structure was observed only in the range $0 \le x \le 0.4$ [76]. The electrical conductivity of $LaMnO_{3\pm\delta}$ and $La_{0.6}Sr_{0.4}MnO_{3-\delta}$ increases regularly with introduction of nickel into the manganese sublattice [76, 82, 91]. Small additions of cobalt ($x \le 0.05$) also lead to increasing conductivity of the $La_{0.6}Sr_{0.4}Mn_{1-x}Co_xO_{3-\delta}$ solid solutions [82]. Thermal expansion of the $(La,Sr)Mn_{1-x}M_xO_{3-\delta}$ (M = Fe, Ni) ceramics is essentially independent of the dopant concentration (Table 7).

Doping $La_{0.6}Sr_{0.4}MnO_{3-\delta}$ with iron or nickel was established to decrease dramatically the ionic conductivity, which is the oxygen permeation flux-limiting factor [75, 85, 92]. Such behavior is determined, probably, by the formation of defect associates like M'_{Mn}–$V_O^{\bullet\bullet}$–M'_{Mn}, where $V_O^{\bullet\bullet}$ is the oxygen ion vacancy and M'_{Mn} refers to the Fe^{2+} and Ni^{2+} ions which are incorporated into the manganese sublattice and formed owing to the oxidation of manganese ions [75, 76]:

$$M_{Mn}^{\times} + Mn_{Mn}^{\times} \rightarrow M'_{Mn} + Mn_{Mn}^{\bullet} \quad (1)$$

with $Mn_{Mn}^{\bullet}$ being the Mn^{4+} ions according to the Kroeger-Vink notation.

The electrochemical activity of the $La_{0.6}Sr_{0.4}Mn_{1-x}M_xO_{3-\delta}$ electrodes in contact with solid electro-

Table 7 Thermal expansion coefficients of $LnMnO_3$-based ceramics

Composition	Averaged TEC values		Ref.
	Temperature range (K)	$\bar{\alpha} \times 10^6$ (K^{-1})	
$LaMnO_3$	320–580	7.7	[64]
	580–1100	11.8	
$La_{0.8}Ca_{0.2}MnO_3$	320–520	6.3	[63]
	550–1050	10.6	
$La_{0.6}Ca_{0.4}MnO_3$	350–1050	9.3	[63]
$La_{0.5}Ca_{0.5}MnO_3$	350–1050	10.7	[63]
$La_{0.8}Sr_{0.2}MnO_3$	340–540	7.7	[64]
$La_{0.6}Sr_{0.4}MnO_3$	320–1100	11.7	[64]
$La_{0.5}Sr_{0.5}MnO_3$	320–1100	12.3	[64]
$La_{0.6}Sr_{0.4}Mn_{0.8}Fe_{0.2}O_3$	300–1100	11.3	[74]
$La_{0.6}Sr_{0.4}Mn_{0.6}Fe_{0.4}O_3$	300–1100	12.0	[74]
$La_{0.6}Sr_{0.4}Mn_{0.5}Fe_{0.5}O_3$	300–1100	12.7	[74]
$La_{0.6}Sr_{0.4}Mn_{0.95}Co_{0.05}O_3$	300–1100	14.3	[82]
$La_{0.6}Sr_{0.4}Mn_{0.95}Ni_{0.05}O_3$	300–1100	14.3	[82]
$La_{0.6}Sr_{0.4}Mn_{0.8}Ni_{0.2}O_3$	350–1100	12.7	[76]
$La_{0.6}Sr_{0.4}Mn_{0.6}Ni_{0.4}O_3$	300–1100	12.5	[76]
$La_{0.8}Pb_{0.2}MnO_3$	300–1100	11.9	[69]
$La_{0.6}Pb_{0.4}MnO_3$	300–1100	9.2	[69]
$NdMnO_3$	750–1100	10.0	[66]
$Nd_{0.8}Ca_{0.2}MnO_3$	550–1200	10.6	[66]
$Nd_{0.6}Ca_{0.4}MnO_3$	500–1200	11.0	[66]
$Nd_{0.5}Ca_{0.5}MnO_3$	500–1200	11.3	[66]
$GdMnO_3$	300–1070	6.3	[65]
$Gd_{0.5}Ca_{0.5}MnO_3$	300–1070	10.0	[65]
$YbMnO_3$	300–1100	8.6	[67]
$Yb_{0.6}Ca_{0.4}MnO_3$	500–700	4.5	[67]
	700–1100	8.0	
$Yb_{0.5}Ca_{0.5}MnO_3$	300–1100	10.2	[67]
$YMnO_3$	620–1100	3.3	[79]
$Y_{0.6}Ca_{0.4}MnO_3$	300–650	1.1	[79]
	600–1100	5.4	
$Y_{0.5}Ca_{0.5}MnO_3$	450–670	3.0	[79]
	670–1100	9.1	

lytes based on stabilized zirconia increases with incorporation of moderate amounts of the transition metals into the B sublattice of the perovskites, as will be considered below.

Oxide materials based on $AMnO_{3-\delta}$ (A = Ca, Sr)

The $CaMnO_{3-\delta}$ phase with the cubic perovskite-type structure was reported to exist within the limits of the Ca/Mn ratio from 0.86 to 1.06 [93]. Here, an excess of Ca and Mn results in separation of the $Ca_4Mn_3O_{10}$ and $CaMn_2O_4$ compounds, respectively; formation of $CaMn_2O_4$ may be also caused by oxygen deficiency [93]. The electrical conductivity of the A-site deficient $Ca_{0.89}MnO_{3-\delta}$ is close to that of stoichiometric $CaMnO_{3-\delta}$, whereas hyperstoichiometric calcium additions were found to lead to a dramatic decrease in the conductivity (by a factor of 10^3 at room temperature). At temperatures above 900 K, the electrical conductivity and Seebeck coefficients of both A-site and B-site deficient perovskites are close to that of the stoichiometric compound [93]. The conductivity of $CaMnO_{3-\delta}$ increases with the incorporation of lanthanum cations into the calcium sublattice [62].

In the pseudobinary system of $CaMnO_3$–$CaTiO_3$ the cubic solid solutions based on the calcium manganite $CaMn_{1-x}Ti_xO_{3-\delta}$ were established to form in the range $0 \le x \le 0.2$, whereas the calcium titanate- based cubic phase of $Ca(Ti,Mn)O_{3-\delta}$ exists at $0.8 \le x \le 1.0$ [78]. Electronic conduction in $CaMn_{1-x}Ti_xO_{3-\delta}$ occurs via small polaron transport between manganese cations. As a result, increasing the titanium content leads to a decrease in the conductivity [78]. According to the results of studying the Seebeck coefficient, all of the $CaMn_{1-x}Ti_xO_{3-\delta}$ ceramics are n-type semiconductors [78].

Formation of perovskite solid solutions is characteristic of $BiMnO_3$–$SrMnO_3$ in the concentration range $0.3 \le x \le 0.7$ [80]; at $x = 0.3$, the crystal structure is cubic. Increasing the strontium content results in the appearance of tetragonal distortions of the crystal lattice, which vanish on heating the oxides [80]. The maximum conductivity was found for the solid solutions with $x = 0.5$–0.6. All the perovskites at temperatures above 500 K are n-type semiconductors, and metallic conductivity was detected at temperatures above 700–800 K. Thermal expansion coefficients of the ceramics were calculated from dilatometric data to be in the range $(9.5–10.0)\times10^{-6}$ K^{-1} at 300–570 K and $(13–14)\times10^{-6}$ K^{-1} at 600–1000 K [80].

Perovskite-type $LnCoO_{3\pm\delta}$

Cobaltites of rare-earth elements and solid solutions based on them are promising materials for electrodes of electrochemical cells with solid electrolytes based on ceria and bismuth oxide [1, 88, 94–96], high-temperature electrochemical membranes [97, 98], cathodes of waveguide CO_2 lasers [99–101], and oxidation catalysts [101]. The attention paid to these perovskites is associated with the high electronic and ionic conductivities of cobaltites, and their noticeable electrochemical and catalytic activity in oxygen-containing environments.

Phase diagrams, selected phase relationships, and thermodynamic properties of the perovskite-type $LnCoO_3$ were reported in publications from the research group at the Ural State University [12, 13, 102–109]. In the binary oxide systems of Ln_2O_3–CoO_x (Ln = Sm, Eu, Gd, Tb, Dy, Ho), only the perovskite phase was found; no Ln_2CoO_4-type phases form in these systems [104]. The phase diagrams of Ln_2O_3–CoO_x with Ln = La, Pr, or Nd are more complex [103, 105]. In particular, two phases were reported in the Pr–Co–O system: perovskite-like $PrCoO_3$ and tetragonal $Pr_4Co_3O_{10}$ [105].

The thermodynamic stability of $LnCoO_3$ decreases with the decreasing REE cation radii [103, 104]. This is caused by an increase of the perovskite lattice

Table 8 Oxygen nonstoichiometry[a] and perovskite phase stability limits[b] of $LnCoO_{3-\delta}$ [108]

Phase	Oxygen nonstoichimetry				ΔS_V° (J/mol K)	$-\Delta H_V^\circ$ (kJ/mol)
	T (K)	$\delta_0 \times 10^2$	$-a$	$K_V \times 10^3$		
$LaCoO_{3-\delta}$	1373	0.635	0.41 ± 0.07	2.65 ± 0.65	83 ± 3	169 ± 5
	1473	1.53	0.55 ± 0.01	6.57 ± 0.12		
$PrCoO_{3-\delta}$	1373	0.472	0.39 ± 0.01	2.57 ± 0.04	163 ± 3	227 ± 5
	1423	1.27	0.33 ± 0.01	7.7 ± 0.1		
	1473	1.99	0.42 ± 0.01	9.50 ± 0.06		
$NdCoO_{3-\delta}$	1373	0.290	0.35 ± 0.02	1.6 ± 0.1	149 ± 3	271 ± 4
	1473	1.05	0.51 ± 0.02	4.27 ± 0.30		
Phase	$\log p'_{O_2} = A + B/T$ (atm)		$\log p''_{O_2} = A + B/T$ (atm)			
	A	$-B \times 10^{-3}$	A	$-B \times 10^{-3}$		
$LaCoO_{3-\delta}$	12.8 ± 0.4	22.5 ± 0.6	6.86 ± 0.08	12.7 ± 0.1		
$PrCoO_{3-\delta}$	10.40 ± 0.04	18.42 ± 0.04	4.9 ± 0.1	10.1 ± 0.2		
$NdCoO_{3-\delta}$	7.31 ± 0.06	14.4 ± 0.1	5.5 ± 0.2	10.6 ± 0.2		

[a] Isothermal dependences of oxygen nonstoichiometry (δ) on oxygen partial pressure are approximated by the equation $\delta = K_V(p_{O_2})$[a]. δ_0 is the nonstoichiometry value in air. ΔS_V° and ΔH_V° are the values of entropy and enthalpy of oxygen vacancy formation, respectively

[b] p'_{O_2} and p''_{O_2} are the equilibrium oxygen pressures of the perovskite phase decomposition according to Eqs. 3 and 4, respectively

distortion (σ_s) expressed in terms of the tolerance factor t:

$$\sigma_s = 1 - t = 1 - \frac{r_{Ln^{3+}} + r_{O^{2-}}}{\sqrt{2}(r_{Co^{3+}} + r_{O^{2-}})} \quad (2)$$

where $r_{O^{2-}}$, $r_{Co^{3+}}$, and $r_{Ln^{3+}}$ are the radii of oxygen, cobalt, and REE ions, respectively. The perovskites with Ln = La, Pr, Nd, Sm, or Eu were ascertained to melt incongruently [12, 13]. Other cobaltites decompose on heating with formation of REE and cobalt oxides, and their melting occurs only after decomposition [13]. The temperatures of melting and decomposition of cobaltites decrease with the decreasing REE radii (Table 1), which is in agreement with the conclusion on the decreasing thermodynamic stability.

The difference in the phase diagrams and stability results in different behavior for $LnCoO_3$ at low oxygen partial pressures. When the oxygen pressure is reduced, decomposition of the cobaltites of lanthanum, praseodymium, and neodymium occurs by the reactions [105, 108]

$$4LnCoO_{3-\delta} \rightleftharpoons Ln_4Co_3O_{10} + \frac{1}{1-y}Co_{1-y}O + \frac{2(1-2\delta)(1-y)-1}{2(1-y)}O_2 \quad (3)$$

$$6LnCoO_{3-\delta} + Ln_2O_3 \rightleftharpoons 2Ln_4Co_3O_{10} + \frac{1-6\delta}{2}O_2 \quad (4)$$

The stability limits of these cobaltites are given in Table 8. The dissociation of $LnCoO_3$ (Ln = Sm, Eu, Gd, Tb, Dy, Ho) at reducing oxygen pressures leads to the formation of ordinary metal oxides directly [102]:

$$2LnCoO_{3-\delta} \rightleftharpoons Ln_2O_3 + 2CoO + \frac{1-2\delta}{2}O_2 \quad (5)$$

As a result, the solid state synthesis in a nitrogen atmosphere was observed not to result in the formation of perovskite-type $LnCoO_3$ with Ln = Sm or Dy [110]. When heating mixtures of oxides of cobalt and either La, Pr, or Nd in the nitrogen atmosphere, the perovskite phases form at 1020–1170 K, while formation of Ln_2CoO_4 was detected at higher temperatures [110].

Specific features of the solid state synthesis of cobaltites were studied in detail [12, 111–114]. The rate of the solid state reaction was pointed out to be limited by diffusion of cobalt and oxygen ions and to decrease with the decreasing radii of the REE cations [12, 111–113]. Analogously to other oxide materials, the temperature of formation of the perovskite phase can be reduced using the techniques of coprecipitation or thermal decomposition of metal nitrates or organic precursors [12, 114].

In contrast to REE manganites, $LnCoO_3$ were established to tend to oxygen hypostoichiometry [99, 101, 108, 115, 116]. The only exception is praseodymium cobaltite, which exhibits oxygen hyperstoichiometry at low temperatures owing to the presence of tetravalent praseodymium cations [115, 116]. The crystal lattice of REE cobaltites is a function of the lanthanide ionic radii, oxygen nonstoichiometry, and the specific electronic structure of the REE cations [115]. While the decreasing lanthanide radii leads to increasing lattice distortion, the effect of increasing the oxygen content has the opposite effect. As a result, the perovskite-type lattice was found to be rhombohedrally distorted for Ln = La, cubic for Ln = Pr and Nd, and orthorhombic for Ln = Sm and Gd [115–121].

The electrical conductivity of $LnCoO_{3-\delta}$ is significantly higher compared to REE manganites [51, 101, 115, 116, 120–130]. Here, the decreasing lanthanide cation radii tends to a decrease in the conductivity and to an increase in the Seebeck coefficient of cobaltites [115, 116, 121, 122]. Since electronic conduction occurs via electron hole transport, a decrease in the oxygen partial pressure

results in a decrease in the conductivity at temperatures above 900 K owing to oxygen leaving the crystal lattice and reducing the charge carrier concentration [115, 117, 122, 124, 131]. The TEC values of the $LnCoO_{3-\delta}$ (Ln = La–Gd) ceramics are given in Table 9.

Oxygen ionic conductivity and permeation fluxes through $LnCoO_{3-\delta}$ membranes were shown to decrease with the decreasing REE cation radii [115–119, 121, 125, 132]. A theoretical model for a qualitative explanation of such behavior was considered [115]. Note that a major contribution to oxygen transport through $LaCoO_{3-\delta}$ ceramics is provided by oxygen diffusion in the ceramic grain boundaries [133]. This effect was demonstrated to be most pronounced for the membranes prepared by the standard ceramic technique when sintering via a liquid phase formation takes place [133]. Extremely prolonged processes of steady-state attainment are characteristic of such ceramics of lanthanum cobaltite and solid solutions based on them after placing the membrane under an oxygen chemical potential gradient [52, 133]. Here, decreasing the grain size of $LaCoO_{3-\delta}$ polycrystalline specimens prepared using organic precursors leads to decreasing oxygen permeability [133].

Table 9 Thermal expansion coefficients of $LnCoO_{3-\delta}$-based ceramics in air

Composition	T (K)	$\bar{\alpha} \times 10^6$ (K^{-1})	Ref.
$LaCoO_{3-\delta}$	300–450	19	[15]
	680–1020	22	[15]
$La_{0.8}Sr_{0.2}CoO_{3-\delta}$	300–1100	18.31	[115]
	300–820	19	[123]
$La_{0.6}Sr_{0.4}CoO_{3-\delta}$	300–1100	18.9	[121]
$La_{0.6}Sr_{0.3}CoO_{3-\delta}$	300–1100	20.8	[134]
$La_{0.5}Sr_{0.5}CoO_{3-\delta}$	300–1100	22.4	[121]
	300–820	18	[123]
$LaCo_{0.8}Cr_{0.2}O_{3-\delta}$	300–1100	23.6	[52]
$LaCo_{0.6}Cr_{0.4}O_{3-\delta}$	300–1100	20.3	[52]
$LaCo_{0.6}Fe_{0.2}Ni_{0.2}O_{3-\delta}$	300–1100	19.2	[135]
$LaCo_{0.5}Fe_{0.2}Ni_{0.3}O_{3-\delta}$	300–1100	18.0	[135]
$LaCo_{0.7}Ni_{0.3}O_{3-\delta}$	300–1100	17.3	[52]
$LaCo_{0.8}W_{0.2}O_{3\pm\delta}$	300–700	10.0	[136]
	700–1100	19	[136]
$LaCo_{0.8}Ga_{0.2}O_{3-\delta}$	300–1130	22.2	[137]
$LaCo_{0.6}Ga_{0.4}O_{3-\delta}$	430–680	18.7	[137]
	680–1100	22.3	[137]
$LaCo_{0.6}Ga_{0.3}Mg_{0.1}O_{3-\delta}$	300–1100	19.8	[138]
$LaCo_{0.4}Ga_{0.4}Mg_{0.2}O_{3-\delta}$	300–1100	15.4	[138]
$La_{0.5}Sr_{0.5}Co_{0.75}Ni_{0.25}O_{3-\delta}$	300–970	14.2	[13]
$La_{0.5}Sr_{0.5}Co_{0.8}Cu_{0.2}O_{3-\delta}$	300–970	19.3	[13]
$PrCoO_{3\pm\delta}$	650–1100	28.3	[125]
$Pr_{0.8}Sr_{0.2}CoO_{3-\delta}$	400–1100	18.3	[125]
$Pr_{0.6}Sr_{0.4}CoO_{3-\delta}$	400–800	19.5	[125]
	850–1100	26.1	[125]
$NdCoO_{3-\delta}$	300–1100	27.9	[127]
$Nd_{0.8}Sr_{0.2}CoO_{3-\delta}$	300–800	20.7	[127]
	800–1100	17.5	[127]
$Nd_{0.6}Sr_{0.4}CoO_{3-\delta}$	300–600	14.5	[127]
	700–1100	21.9	[127]
$Nd_{0.8}Ca_{0.2}CoO_{3-\delta}$	300–1100	17.1	[127]
$SmCoO_{3-\delta}$	800–1150	22.5	[121]
$Sm_{0.8}Sr_{0.2}CoO_{3-\delta}$	650–1100	20.1	[121]
$Sm_{0.6}Sr_{0.4}CoO_{3-\delta}$	300–900	17.09	[121]
	900–1100	28.7	[121]
$GdCoO_{3-\delta}$	800–1100	23.6	[128]

A-site-substituted cobaltites (Ln,A)$CoO_{3-\delta}$ (A = Sr, Ca, Ba, Pb, Bi)

Similar to the perovskite oxides considered above, the electronic and ionic conductivities of cobaltites as well as their electrochemical activity increase drastically with incorporating divalent metal cations into the A sublattice [51, 95, 115, 118, 121, 140–142].

The concentration range for forming solid solutions in the $La_{1-x}A_xCoO_{3-\delta}$ systems was reported to be $0 \le x \le 0.7$ for A = Sr [115, 123], $0 \le x \le 0.6$ for A = Ba [143], $0 \le x \le 0.25$ for A = Pb [144], and $0 \le x \le 0.10$ for A = Bi [142, 145]. The thermodynamic and thermal stabilities of lanthanum cobaltites decrease with the alkaline earth element dopant additions [107, 124]. The decomposition of the $La_{1-x}Sr_xCoO_{3-\delta}$ solid solutions at reducing oxygen partial pressures was established to occur by the reaction [101, 107]

$$2La_{1-x}Sr_xCoO_{3-\delta_1} \rightleftharpoons (La_{1-x}Sr_x)_2CoO_{4+\delta_2} + \frac{1}{1-y}Co_{1-y}O + \frac{1}{2}\left(2 - 2\delta_1 - \delta_2 - \frac{1}{1-y}\right)O_2 \quad (6)$$

which differs considerably from the undoped lanthanum cobaltite decomposition process expressed by Eqs. 3 or 4. Table 10 lists the stability limits and thermodynamic data for Eq. 6. At further decreases in oxygen pressure, one can observe reduction of the formed cobalt oxide to metal and then reducing solid solutions of $(La,Sr)_2CoO_{4+\delta}$ with the K_2NiF_4-type structure, forming oxides of lanthanum and strontium as well as metallic cobalt [101].

The dopant concentration limits of existing single-phase $Ln_{1-x}Sr_xCoO_{3-\delta}$ (Ln = Pr, Nd, Sm) perovskites are close to that of the $La_{1-x}Sr_xCoO_{3-\delta}$ system [1, 115]. For $Gd_{1-x}A_xCoO_{3-\delta}$ (A = Sr, Ca) the range of formation of the solid solutions with the orthorhombic perovskite-type structure was ascertained to be $0 \le x \le 0.15$, whereas co-existing orthorhombic and cubic perovskite phases were observed at higher alkaline earth element additions [115, 128].

Oxygen nonstoichiometry of the $La_{1-x}Sr_xCoO_{3-\delta}$ solid solutions has been studied in detail [99–101, 146]. The data on the nonstoichiometry of $La_{0.7}Sr_{0.3}CoO_{3-\delta}$,

Table 10 Standard free energy of the Eq. 6 and stability limits of $La_{1-x}Sr_xCoO_{3-\delta}$ at 1273 K [107]

x	ΔG^0 (J/mol) (1273–1473 K)	$p_{O_2}^{\text{decomposition}}$ (atm) (1273 K)
0.1	−(179480 ± 11000) + (97.35 ± 1.90) × T (± 500)	3.2×10^{-5}
0.2	−(176700 ± 3350) + (99.65 ± 0.57) × T (± 200)	7.0×10^{-5}
0.3	−(88730 ± 2680) + (33.63 ± 0.37) × T (± 130)	7.0×10^{-4}

determined by coulometric titration and reduction in a hydrogen atmosphere, differ to a considerable extent from the results of iodometric titration (Table 11). This was explained by a possible existence of O^- ions in the perovskite lattice at low temperatures, along with heterogeneity of the cobaltite at reduced oxygen pressures owing to its partial decomposition according to the Eq. 6 [101]. The variation in the oxygen nonstoichiometry of powders and ceramics of $La_{0.7}Sr_{0.3}CoO_{3-\delta}$ was also mentioned [101]. The values of the heat capacity of the $La_{1-x}Sr_xCoO_{3-\delta}$ ($x = 0$–0.3) solid solutions in the temperature range from 300 to 1100 K were found to be close to each other [147].

Analogously to other perovskites, doping with alkaline earth metal cations results in an increase in the Co^{4+} concentration and electrical conductivity of $Ln_{1-x}A_xCoO_{3-\delta}$ [101, 115, 118, 121, 123, 146]. In particular, a transition to metallic conductivity is observed for the $Ln_{1-x}Sr_xCoO_{3-\delta}$ (Ln = La, Pr, Nd, Sm) solid solutions in air at $x \geq 0.3$ [115, 121]. The conductivity of the substituted gadolinium cobaltite was measured to be substantially lower, caused by the non-single-phase composition of the ceramics [128, 129]. Electrical properties of the $La_{1-x}Ba_xCoO_{3-\delta}$ system are close to those of the strontium-doped cobaltites [143]. Introducing cation vacancies or bismuth cations into the A sublattice leads to decreasing conductivity [134, 142, 145].

Under a reducing oxygen pressure, the Co^{4+} ion concentration in $Ln_{1-x}Sr_xCoO_{3-\delta}$ decreases and the crystal field near the cobalt ions distorts, which leads to the appearance of trapping levels and a decrease in the conduction band [101, 115, 117, 119]. As a result, the conductivity of the solid solutions decreases. The formation of the defect associates between oxygen vacancies and strontium ions is assumed to explain the electrical and magnetic properties of the cobaltites [146]. The ferromagnetic Curie temperature and magnetic moment of $La_{1-x}Sr_xCoO_{3-\delta}$ were found to increase with increasing tetravalent cobalt concentration [101, 146]. The catalytic activity of cobaltites in the CO oxidation reaction is also proportional to the Co^{4+} content [101].

The dopant concentration dependences of the oxygen permeability and ionic conductivity in $Ln_{1-x}A_xCoO_{3-\delta}$ have a complex nature, being determined by both oxygen nonstoichiometry and cobalt ion oxidation state [115–118, 132]. The ionic conductivity was ascertained to decrease with the decreasing mean radii of the A-site cations [117, 148]. Compared to the strontium-substituted cobaltites, the oxygen permeability of perovskites doped with Ca, Pb, or Bi is noticeably lower [97, 132]. Creation of cation vacancies in either A or B sublattices leads to decreasing oxygen permeability [148]. Increasing the strontium content in $Ln_{1-x}Sr_xCoO_{3-\delta}$ was found to result in a definite decrease in the ionic conductivity at small dopant additions ($x \leq 0.2$), whereas further doping provides a sharp increase in the oxygen ionic transport [115–118]. Among cobaltites of REE and strontium, the maximum oxygen permeability was established for the solid solutions $La_{1-x}Sr_xCoO_{3-\delta}$ with $x = 0.65$–0.70 [97, 115–117, 148, 149]. Some results of studying oxygen permeation are presented in Table 12. The values of specific oxygen permeability $J(O_2)$ (mol s^{-1} cm^{-1}) were

Table 11 Oxygen nonstoichiometry of $La_{0.7}Sr_{0.3}CoO_{3-\delta}$

T (K)	p_{O_2} (atm)	δ	Measurement method[a]	Ref.
770	0.21	0.030 ± 0.003	HR	[146]
		0.023 ± 0.002	IT	[146]
923	0.21	0.013	IT	[101]
		0.017	CT	[101]
1193	0.21	0.008	IT	[101]
		0.0179	CT	[101]
	0.06	0.022	IT	[101]
		0.0286	CT	[101]
	0.014	0.040	IT	[101]
		0.0462	CT	[101]
	0.002	0.037	IT	[101]
		0.0729	CT	[101]
1170	0.21	0.075	TGA	[99]
1270	0.21	0.094	TGA	[99]
1370	0.21	0.122	TGA	[99]
1420	0.21	0.139	TGA	[99]

[a] HR, IT, CT, and TGA refer to the reduction in a hydrogen atmosphere, iodometric titration, coulometric titration, and thermal gravimetry, respectively

Table 12 Oxygen permeability of $Ln_{1-x}A_xCoO_{3-\delta}$ ceramics at 1100 ± 5 K (p_2 = 0.21 atm, d = 2.7–3.0 mm) [115]

Ln	A	x	p_1 (atm)	$J(O_2) \times 10^{10}$ (mol s^{-1} cm^{-1})
La	Sr	0	0.13	2.0×10^2
			8.0×10^{-2}	2.9×10^2
		0.2	0.13	28
			3.7×10^{-2}	1.5×10^2
		0.4	2.9×10^{-3}	2.8×10^2
		0.5	0.13	3.4×10^2
		0.7	0.14	3.6×10^2
			4.13×10^{-2}	4.3×10^2
		0.8	0.13	4.6×10^2
			8.3×10^{-2}	3.6×10^2
		1.0	0.16	2.3×10^2
			2.3×10^{-2}	2.0×10^2
	Pb	0.2	0.14	93
			4.3×10^{-2}	1.1×10^2
	Bi	0.1	4.1×10^{-2}	2.9
Pr	Sr	0	0.19	1.7×10^2
			2.2×10^{-3}	89
		0.1	0.13	2.1×10^2
			6.9×10^{-3}	1.5×10^2
		0.2	6.9×10^{-2}	91
			2.7×10^{-3}	1.2×10^2
		0.3	5.4×10^{-2}	76
			1.8×10^{-3}	89
		0.4	0.15	59
			1.9×10^{-3}	87
Nd	Sr	0.2	0.11	87
			4.2×10^{-3}	62
		0.3	0.16	76
			4.6×10^{-3}	48
		0.4	0.14	11
	Ca	0.1	7.6×10^{-2}	20

calculated by the equation [150]:

$$J(O_2) = j \cdot d \cdot \left[\ln \frac{p_2}{p_1}\right]^{-1} \quad (7)$$

where j (mol s^{-1} cm^{-2}) is the permeation flux density, d is the membrane thickness, and p_1 and p_2 are the oxygen partial pressures at the membrane permeate side and feed side, respectively ($p_2 > p_1$).

The solid solutions (La,A)(Co,M)$O_{3-\delta}$ (M = Ti, Mn, Fe, Ni, Cu, Ga, Mg)

For the B-site substituted cobaltites, the main regularities of the property variations are close to those typical for manganites and chromites of the rare-earth elements. In particular, the concentration range of existing solid solutions of Ln(Co,M)$O_{3-\delta}$ is determined by the thermodynamic possibilities of formation of the $LnMO_3$ perovskite phase at given conditions. Incorporating divalent cations into the A sublattice leads typically to decreasing thermodynamic stability of the perovskite phases and a narrowing of the concentration range for forming B-site-substituted solid solutions.

The limits of existence of the $LaCo_{1-x}Ti_xO_{3\pm\delta}$ perovskites, synthesized at 1670–1720 K in air, were determined to be $0 \le x \le 0.5$ [151]. In this system, no oxygen hyperstoichiometric phases form and insertion of excessive oxygen into the perovskite lattice leads to the appearance of phase impurities. Oxygen hyperstoichiometry was determined by the iodometric method not to exceed 0.02, which is within the experimental error limits [151]. Doping by titanium results in an increase in divalent cobalt concentration [151]. Creation of cation vacancies in the A sublattice enlarges the range of the solid solution formation: the single perovskite phase of $La_{1-y}Co_{1-x}Ti_xO_{3-\delta}$ was observed to exist within the limits $0 \le x \le 0.7$, $0 \le y \le 0.23$, and $0 \le \delta \le 0.25$ [151]. The lower limit corresponds approximately to the composition $(1-x)LaCoO_3$–$xLa_{2/3}TiO_3$. Owing to reducing the average oxidation degree of cobalt ions, the electrical conductivity decreases dramatically with addition of titanium [151].

Properties of the La(Co,Cr)O_3 solid solutions [15, 17, 47, 52] were reviewed briefly above. Similar to doping cobaltites by chromium, doping with manganese leads to decreasing conductivity of (La,A)$Co_{1-x}Mn_xO_{3-\delta}$ (A = Ca, Pb) [152–154]. When adding magnesia to such materials, separation of a cobalt-magnesium spinel phase and a further decrease in conductivity were observed [153, 154].

In the $LaCo_{1-x}Ni_xO_{3-\delta}$ system, perovskite-type solid solutions form in the range $0 \le x \le 0.5$ [155]. Incorporation of strontium into the lanthanum sublattice results in increasing oxygen nonstoichiometry and decreasing thermodynamic stability, and the perovskite phase of $La_{0.5}Sr_{0.5}Co_{1-x}Ni_xO_{3-\delta}$ exists only at $x < 0.25$ [139]. In both cases, any further increase in the nickel content leads to separation of a K_2NiF_4-like phase of La_2NiO_4 and nickel oxide [139, 155]. The conductivity of lanthanum cobaltite increases and the thermal expansion decreases with additions of nickel [52, 155]. Despite increasing oxygen vacancy concentration, the ionic conductivity of $LaCo_{1-x}Ni_xO_{3-\delta}$ decreases with x [52]. The probable reason for such behavior is formation of the defect associates similar to $La_{0.6}Sr_{0.4}Mn_{1-x}Ni_xO_{3-\delta}$ (see above).

The solid solutions of $La_{0.5}Sr_{0.5}Co_{1-x}Cu_xO_{3-\delta}$ were found to exist at $x \le 0.20$ [139]. It was mentioned that copper addition allows improvement of the mechanical strength and sinterability of the cobaltite ceramics, caused by the sintering mechanism via formation of a liquid phase at the ceramic grain boundaries [139].

For the pseudobinary oxide system $(1-x)LaCoO_{3-\delta}$–$xLaGaO_3$, forming the single perovskite phase was established within all the substitution range of $0 \le x \le 1.0$ [137]. Both electronic conductivity and oxygen permeability of lanthanum cobaltite decrease when cobalt is substituted for gallium [137]. Here, further doping of La(Co,Ga)$O_{3-\delta}$ solid solutions with magnesium was demonstrated to lead to an increase in both oxygen vacancy and Co^{4+} ion concentrations, which results in increasing ionic and electronic conduction [138]. The maximum solid solubility of magnesium in the B sublattice of $LaCo_{1-x-y}Ga_xMg_yO_{3-\delta}$ perovskites increases with gallium content from $y = 0.10$ to 0.25. The data on thermal expansion and oxygen permeability of the La(Co,Ga,Mg)$O_{3-\delta}$ solid solutions are given in Tables 9 and 13.

Perovskite-like oxides based on $SrCoO_{3-\delta}$

Perovskite-like phases based on strontium cobaltite, $SrCoO_{3-\delta}$, having high ionic conductivity with prevailing electronic conductivity are of great interest for high-purity oxygen separation membranes [97, 115, 132, 148]. On the other hand, the electrical conductivity and electrochemical activity of the $SrCoO_{3-\delta}$-based oxides in contact with the solid electrolytes based on bismuth oxide were mentioned to be lower compared to the solid solutions of $Ln_{1-x}Sr_xCoO_{3-\delta}$ [95, 115, 158].

Strontium cobaltite is characterized by a large oxygen nonstoichiometry δ, which may achieve 0.75 [159, 160]. This oxide can form a number of perovskite-related phases, depending on the oxygen content [115]. At low temperatures in air, the crystal structure of $SrCoO_{3-\delta}$ was reported to be tetragonal [158, 161] or hexagonal [162]. The oxygen ionic conductivity of strontium cobaltite depends very weakly on temperature at 970–1100 K and increases with increasing oxygen partial pressure [148, 160, 161, 163–165]. As the structure of $SrCoO_{3-\delta}$ is distorted compared to the cubic perovskite, the ionic conductivity and oxygen permeability of

Table 13 Oxygen permeation flux density through perovskite oxide membranes at 1223 ± 4 K (p_2 = 0.21 atm, d = 1.00 ± 0.02 mm)

Membrane	Phase composition[a]	$p_1 \times 10^2$ (atm)	j (mol s^{-1} cm^{-2})	Ref.
$LaCo_{0.8}Fe_{0.1}Ni_{0.1}O_{3-\delta}$	R	3.1	1.1×10^{-9}	[135]
$LaCo_{0.7}Fe_{0.1}Ni_{0.2}O_{3-\delta}$	R	9.5	3.2×10^{-9}	[135]
$LaCo_{0.6}Fe_{0.2}Ni_{0.2}O_{3-\delta}$	R	3.1	1.2×10^{-9}	[135]
$LaCo_{0.5}Fe_{0.2}Ni_{0.3}O_{3-\delta}$	R	9.5	3.1×10^{-9}	[135]
$LaCo_{0.4}Ga_{0.4}Mg_{0.2}O_{3-\delta}$	R	2.1	6.1×10^{-8}	[138]
$LaCo_{0.6}Ga_{0.3}Mg_{0.1}O_{3-\delta}$	R	2.1	6.6×10^{-9}	[138]
$LaGa_{0.8}Ni_{0.2}O_{3-\delta}$	R	2.1	3.4×10^{-8}	[156]
$LaGa_{0.7}Ni_{0.3}O_{3-\delta}$	R	2.1	3.5×10^{-8}	[156]
$LaGa_{0.6}Ni_{0.4}O_{3-\delta}$	R	2.1	6.3×10^{-8}	[156]
$LaGa_{0.5}Ni_{0.5}O_{3-\delta}$	R	2.1	6.6×10^{-8}	[156]
$LaGa_{0.4}Ni_{0.6}O_{3-\delta}$	R + I	2.1	1.9×10^{-8}	[156]
$LaFe_{0.8}Ni_{0.2}O_{3-\delta}$	C	2.1	4.3×10^{-10}	[157]
$LaFe_{0.7}Ni_{0.3}O_{3-\delta}$	R	2.1	2.8×10^{-9}	[157]
$LaFe_{0.6}Ni_{0.4}O_{3-\delta}$	R	2.1	5.7×10^{-9}	[157]
$LaFe_{0.5}Ni_{0.5}O_{3-\delta}$	O	2.1	8.6×10^{-9}	[157]

[a] C, R, and O refer to the cubic, rhombohedral, and orthorombic single perovskite phase, respectively. R + I means the presence of phase impurities with the main rhombohedrally distorted perovskite phase

strontium cobaltite is considerably lower in comparison with perovskites such as $La_{0.3}Sr_{0.7}CoO_{3-\delta}$ [115–119]. The electronic conduction in $SrCoO_{3-\delta}$, provided by electron hole transport, was stated to decrease in line with decreasing oxygen pressure [115, 162, 164].

A series of research papers [148, 158, 161, 166–177] was devoted to studying physicochemical and electrochemical properties of the solid solutions of $SrCo_{1-x}M_xO_{3-\delta}$ (M = Ti, Cr, Mn, Fe, Ni, Cu, V) and $SrCo_{1-x-y}Fe_xM_yO_{3-\delta}$ (M = Cr, Cu). It was demonstrated that a decrease in the oxygen nonstoichiometry of $Sr(Co,M)O_{3-\delta}$, caused by doping with cations of higher valency in comparison with cobalt (M = Ti, Cr, Mn, Fe), within the limits of the existing single perovskite phase, leads to increasing oxygen permeability and electrical conductivity [167–170, 173]. The effect of introducing cations with the lower valency (M = Cu, Ni) into the cobalt sublattice is the opposite, whereas stabilization of the cubic phase is not typically observed in this case. At ceramic membrane thickness values less than 2 mm and permeate-side oxygen pressures below 0.21 atm, the oxygen permeation fluxes through most of the $SrCoO_{3-\delta}$-based ceramic materials were ascertained to be limited by the oxygen surface exchange rate [148, 173, 176, 177]. The limiting effect of the oxygen exchange rate at the membrane permeate-side surface was shown to be substantially higher compared to the feed-side surface [176]. Increasing the oxygen pressure up to $p_1 \approx 1$ atm and $p_2 = 1$–100 atm results in changing the permeation flux-determining stage, and oxygen fluxes at high oxygen pressures are limited by the oxygen ionic conductivity of the ceramics [178].

Among the perovskite oxides, the maximum oxygen permeability is characteristic of the solid solutions of $SrCo_{1-x}Fe_xO_{3-\delta}$ with $x = 0.20$–0.35 [97, 115, 132, 158, 166]. The poor mechanical properties were noted to be typical for the ceramics of this composition, which may be improved within certain limits by the introduction of chromium or copper into the B sublattice of the perovskites [158, 176]. For the $SrCoO_{3-\delta}$-based ceramics, decreasing ceramic grain size leads to decreasing oxygen permeability, owing to increasing grain-boundary area and its resistance to ionic transport [176, 177]. Selected results on oxygen permeation and thermal expansion of $SrCoO_{3-\delta}$-based materials are given in Tables 14 and 15.

Perovskite-type $LnNiO_{3-\delta}$ and solid solutions based on them

The thermodynamic stability of perovskite phases in the systems Ln–M–O (M is transition metal) in air decreases regularly in the sequence Cr → Ni, which corresponds to the decreasing degree of oxidation of the transition metal cations at atmospheric oxygen pressure. In the ternary systems Ln–Cu–O there generally exist no perovskite phases at oxygen pressures close to atmospheric [179–182]. For the Ln–Ni–O systems, perovskite

Table 14 Oxygen permeation flux density through $SrCoO_{3-\delta}$-based membranes at 1153 ± 4 K (d = 1.40 ± 0.02 mm, p_2 = 0.21 atm, p_1 = 0.084 atm)

Membrane	Phase composition[a]	j (mol s^{-1} cm^{-2})	Ref.
$Sr_{0.70}La_{0.30}CoO_{3-\delta}$	C	2.6×10^{-7}	[171]
$Sr_{0.70}Nd_{0.30}CoO_{3-\delta}$	C	1.6×10^{-7}	[171]
$Sr_{0.70}Sm_{0.30}CoO_{3-\delta}$	C	1.0×10^{-7}	[171]
$Sr_{0.70}Gd_{0.30}CoO_{3-\delta}$	C	4.1×10^{-8}	[171]
$Sr_{0.65}La_{0.35}CoO_{3-\delta}$	C	2.8×10^{-7}	[148]
$Sr_{0.60}La_{0.35}CoO_{3-\delta}$	C	2.0×10^{-7}	[148]
$Sr_{0.55}La_{0.35}CoO_{3-\delta}$	C	1.7×10^{-7}	[148]
$Sr_{0.65}La_{0.35}Co_{0.90}O_{3-\delta}$	C + I	2.5×10^{-7}	[148]
$SrCo_{0.89}Fe_{0.10}Cr_{0.01}O_{3-\delta}$	C + I	4.7×10^{-7}	[176]
$SrCo_{0.85}Fe_{0.10}Cr_{0.05}O_{3-\delta}$	C	5.2×10^{-7}	[176]
$SrCo_{0.95}Ti_{0.05}O_{3-\delta}$	C	4.5×10^{-7}	[173]
$SrCo_{0.80}Ti_{0.20}O_{3-\delta}$	C	4.8×10^{-7}	[173]

[a] C corresponds to the single perovskite-type cubic phase; C + I refers to the cubic perovskite phase with phase impurities

Table 15 Thermal expansion coefficients of perovskite-type oxide ceramics

Composition	T (K)	$\bar{\alpha} \times 10^6$ (K^{-1})	Ref.
$Sr_{0.70}La_{0.30}CoO_{3-\delta}$	300–640/640–1020	19.6 ± 0.5/28.8 ± 0.5	[171]
$Sr_{0.70}Nd_{0.30}CoO_{3-\delta}$	300–640/640–1020	17.1 ± 0.6/31.5 ± 0.5	[171]
$Sr_{0.70}Sm_{0.30}CoO_{3-\delta}$	300–640/640–1020	15.2 ± 0.1/25.9 ± 0.1	[171]
$Sr_{0.70}Gd_{0.30}CoO_{3-\delta}$	300–640/640–1020	13.0 ± 0.1/20.4 ± 0.2	[171]
$Sr_{0.65}La_{0.35}CoO_{3-\delta}$	300–840/840–1100	20 ± 2/27.9 ± 0.6	[148]
$Sr_{0.60}La_{0.35}CoO_{3-\delta}$	300–1100	22 ± 1	[148]
$Sr_{0.55}La_{0.35}CoO_{3-\delta}$	300–1100	18 ± 1	[148]
$Sr_{0.65}La_{0.35}Co_{0.90}O_{3-\delta}$	300–1100	16.9 ± 0.9	[148]
$SrCo_{0.89}Fe_{0.10}Cr_{0.01}O_{3-\delta}$	300–800/800–1080	15.8 ± 0.7/30.5 ± 0.9	[176]
$SrCo_{0.85}Fe_{0.10}Cr_{0.05}O_{3-\delta}$	300–840/840–1080	17 ± 1/29.3 ± 0.9	[176]
$SrCo_{0.95}Ti_{0.05}O_{3-\delta}$	300–750/800–1100	13.1 ± 0.6/28.0 ± 0.8	[173]
$SrCo_{0.80}Ti_{0.20}O_{3-\delta}$	300–700/800–1100	18.3 ± 0.7/28.3 ± 0.9	[173]
$LaGa_{0.8}Ni_{0.2}O_{3-\delta}$	300–1100	10.8 ± 0.1	[156]
$LaGa_{0.6}Ni_{0.4}O_{3-\delta}$	300–1100	11.6 ± 0.3	[156]
$LaGa_{0.5}Ni_{0.5}O_{3-\delta}$	300–1100	11.4 ± 0.3	[156]
$LaGa_{0.4}Ni_{0.6}O_{3-\delta}$	300–1100	11.3 ± 0.1	[156]
$LaFe_{0.8}Ni_{0.2}O_{3-\delta}$	300–1100	8.9 ± 0.1	[157]
$LaFe_{0.6}Ni_{0.4}O_{3-\delta}$	300–1100	10.6 ± 0.3	[157]
$LaFe_{0.5}Ni_{0.5}O_{3-\delta}$	300–1100	11.9 ± 0.1	[157]

phases exist only within a limited range of temperatures and oxygen pressures [183–186]. This results in considerable limitations to the applicability of perovskite-like nickelates, which may be used as electrodes or oxygen membranes only at relatively high oxygen chemical potentials and temperatures below 970 K. In some cases, doping nickelates into the B sublattice allows enlargement of the stability field of the perovskite phase.

Phase diagrams, selected phase relationships, and crystal structures of some Ln–Ni–O phases have been studied [183–192]. The perovskite phase of $LaNiO_{3-\delta}$ was established to be thermodynamically stable at $p_{O_2} \leq 1$ atm only at temperatures below 1170 K [183]. The perovskite-type lanthanum nickelates can be synthesized either by annealing the products of hydroxide coprecipitation or nitrate decomposition in air at 970–1170 K, or by annealing the ceramics, sintered earlier, in an oxygen atmosphere at 1370 K [184–186]. $LaNiO_{3-\delta}$ exhibits metallic conductivity, which is as high as 1.1×10^3 S/cm at room temperature [185].

Since the general tendency for the $LnMO_{3-\delta}$ perovskites is to decreasing thermodynamic stability with decreasing REE cation radii, preparation of the perovskite phases of other rare-earth elements is significantly hampered even in comparison with lanthanum nickelate. As a result, there are very limited data on their synthesis and properties in the literature. In particular, $NdNiO_{3-\delta}$ with the orthorombically distorted perovskite-type structure can be prepared only by annealing the products of hydroxide coprecipitation with potassium chlorate at 970 K [184].

The properties of the pseudobinary systems of $LaNiO_{3-\delta}$–$LaMO_{3-\delta}$ (M = Cr, Mn, Co) were briefly considered above. Similar to these systems, the solid solutions of $LaM_{1-x}Ni_xO_{3-\delta}$ (M = Fe, Ga) form in the approximate range a $0 \leq x \leq 0.5$ [156, 157]. There are also published data on the $La(Al,Ni)O_{3-\delta}$ solid solutions [193]. For all such perovskites, nickel cations were found to be predominantly in the trivalent high-spin state [156, 157, 193]. Increasing the nickel concentration in these perovskites leads to increasing oxygen vacancy concentration and ionic conductivity, which is the limiting factor of oxygen permeation [156, 157]. Correspondingly, the permeation fluxes through ceramic membranes of such oxides increase with increasing nickel content (Table 13).

Results on the structure and physicochemical properties of perovskite-like $LaNi_{0.5}M_{0.5}O_{3\pm\delta}$ (M = Zr, Sn) and $LaNi_{0.75}M_{0.25}O_{3\pm\delta}$ (M = Mo, W) have been published [194, 195]. These perovskites were reported to be p-type semiconductors, stable in air within a wide temperature range (up to 1770 K). Chemical analysis showed that divalent nickel cations exist predominantly in such phases, while formation of a small impurity of Ni^{3+} leads to the oxygen hyperstoichiometry [195].

K_2NiF_4-type oxide compounds

The K_2NiF_4-type rare-earth complex oxides, A_2BO_4, consist of alternating layers of ABO_3 perovskite and AO rock-salt structures along the c-axis [1]. Such oxides are of interest as materials for oxygen electrodes for various solid electrolyte devices. This is associated, primarily, with a sufficiently high electronic conductivity of the $Ln_2MO_{4\pm\delta}$ (M = Co, Ni, Cu) compounds and solid solutions based on them. Although the electrical conductivity of such compounds is lower as compared to their perovskite oxide homologs, the K_2NiF_4-type compounds are most stable in the Ln–M–O systems with M = Ni or Cu in air [179–185]. In addition, some K_2NiF_4-type solid solutions were found to exhibit noticeably high ionic conductivity and oxygen permeability [196, 197], which permits their use as oxygen membrane materials.

One should note also that oxides based on Ln_2MO_4 (M = Co, Ni) refers to the products of decomposition of

the respective perovskite phases at reduced oxygen pressures [101, 107, 183–185]. The conditions in which the K_2NiF_4-type oxides can be formed from the perovskites correspond to those at the permeate side of the oxygen membranes for partial oxidation of hydrocarbons. The K_2NiF_4-type phases, formed owing to the reducing permeate-side surface layers of the perovskite oxidation membranes, are expected to determine the oxygen permeation flux through the membrane. Therefore, studying phases with the K_2NiF_4 structure is of interest for developing ceramic mixed-conductive membranes.

La_2CoO_4 and the solid solutions $(La,A)_2CoO_4$

As mentioned above, the formation of Ln_2CoO_4 phases is typical only for rare-earth cations with large radii (Ln = La, Pr, Nd) [102, 104, 110]. Most of such compounds tend to oxygen hyperstoichiometry. In particular, the homogeneity range of $La_{1.4}Sr_{0.6}CoO_{4+\delta}$ was determined by the coulometric titration method at 1383 K to correspond to δ values from 0.09 to 0.36 [101]. A considerable hysteresis in oxygen partial pressures corresponding to the "perovskite $\leftrightarrow$ K_2NiF_4-type phase" transition was ascribed to diffusion limitations of the cobalt cation transport between the phases [101].

Formation of the $La_{2-x}Sr_xCoO_4$ solid solutions was established in the range $0 \le x \le 1$ [198]. In the $La_{2-x}Ba_xCoO_4$ system the solid solutions were reported to form at $0 \le x \le 0.7$ [198]. For both of these systems the single-phase oxides at $x < 0.3$ can be obtained only in an inert atmosphere, whereas some of the K_2NiF_4-type solid solutions at higher x values may be prepared in air at temperatures below 1370 K [51, 186, 198]. All cobaltites with the K_2NiF_4 structure were stated to be p-type semiconductors [51, 198].

Oxide materials based on Ln_2NiO_4

Properties of $La_2NiO_{4+\delta}$ with the tetragonal K_2NiF_4-type structure and the $La_{2-x}A_xNiO_{4\pm\delta}$ (A = Ca, Sr, Ba) solid solutions have been reported by Kononyuk et al. [197, 199–202]. The concentration ranges of existing solid solutions are $0 \le x \le 1.4$ for A = Sr, $0 \le x \le 1.0$ for A = Ba, and $0 \le x \le 0.5$ for A = Ca [199–201]. When doping with strontium, the conductivity of the ceramics increases and becomes metallic at $x = 1.0$ [199]. Lanthanum nickelate, $La_2NiO_{4+\delta}$, and the solid solutions with moderate alkaline-earth dopant concentration were ascertained to exhibit oxygen hyperstoichiometry in air, while all the solid solutions of $La_{2-x}Sr_xNiO_{4\pm\delta}$ at $x \ge 1.0$ are hypostoichiometric [197, 201, 202]. Reducing the oxygen partial pressure leads regularly to a decrease in the conductivity of the ceramics. The TEC values of the nickelates are $(12–13) \times 10^{-6}\,K^{-1}$ at 300–900 K [200].

For the systems $(1-x)La_2NiO_4-xSr_2TiO_4$ and $(1-x)LaSrNiO_{4-\delta}-xSr_2TiO_4$, formation of solid solutions was reported within the concentration range $0 \le x \le 1$ [203]. Electronic conduction in such oxides occurs via hopping electron holes between the nickel cations. The oxygen content in $(1-x)La_2NiO_4-xSr_2TiO_4$ was determined to be close to stoichiometric [203]. In contrast, only 12–53% of nickel ions in the solid solutions of $(1-x)LaSrNiO_{4-\delta}-xSr_2TiO_4$ are trivalent, resulting in significant oxygen hypostoichiometry [203].

Among other interesting research projects, one can list the results on electrical conductivity of $Nd_2NiO_{4+\delta}$ with additions of nickel oxide [204], the data on the $LaSrNi_xAl_{1-x}O_{4-\delta}$ solid solutions [205], and a series of publications on the $Ln_4Ni_3O_{10}$ (Ln = La, Pr, Nd) phases and solid solutions based on them [190, 206–208]. Table 16 lists the electrical conductivity of selected Ln–Ni–O compounds.

Cuprates of rare-earth elements

Phase diagrams, thermodynamic properties of selected phases in the Ln–Cu–O oxide systems, and their crystal structure have been studied [179–182, 209–214]. In these systems the Ln_2CuO_4 and $Ln_2Cu_2O_5$ phases are most stable in air [179–182, 209, 210]. The thermodynamic stability of Ln_2CuO_4 decreases with the decreasing REE cation radii similar to the perovskite-type oxides, while the opposite behavior is characteristic of $Ln_2Cu_2O_5$ [209, 210]. On reducing the oxygen pressure, the Ln_2CuO_4 (Ln = Pr, Nd, Sm, Eu) phase at 1070–1400 K and the La_2CuO_4 phase at 1180–1400 K were shown to decompose, forming $LnCuO_2$ and REE oxide [179–181]. Here, the decomposition of La_2CuO_4 (1070–1180 K) and Gd_2CuO_4 (1090–1350 K) results directly in the formation of binary metal oxides [181]. Corresponding to the varying free energy of formation, the thermal

Table 16 Electrical conductivity of selected oxide compounds containing nickel and rare-earth elements

Composition	Conductivity (S/cm)		Ref.
	300 K	900 K	
$LaNiO_3$	5.8×10^2	4.1×10^2	[185]
$LaNi_{0.5}Mn_{0.5}O_3$	10	2.8×10^{-2}	[91]
$LaNi_{0.5}Co_{0.5}O_3$	8.7×10^2	8.8×10^2	[155]
$LaNi_{0.5}Ga_{0.5}O_3$	8.4	25	[156]
$LaNi_{0.5}Zr_{0.5}O_3$	0.12	35	[195]
$LaNi_{0.5}Sn_{0.5}O_3$	–	13	[195]
$La_4Ni_3O_{10}$	1.5×10^2	65	[206]
$La_{1.8}Ca_{0.2}NiO_4$	40	77	[200]
$La_{1.5}Ca_{0.5}NiO_4$	28	69	[200]
$LaSrNiO_4$	2.2×10^2	1.3×10^2	[201]
$LaSrNi_{0.5}Ti_{0.5}O_4$	2.3×10^{-4}	0.17	[203]
$La_{0.6}Sr_{1.4}NiO_4$	2.6×10^2	1.2×10^2	[201]
$La_{0.6}Sr_{1.4}Ni_{0.4}Ti_{0.6}O_4$	1.4×10^{-4}	0.12	[203]
$La_{0.5}Sr_{1.5}Ni_{0.5}Ti_{0.5}O_4$	1.7×10^{-3}	0.84	[203]
$La_{1.5}Ba_{0.5}NiO_4$	13	47	[200]
$LaBaNiO_4$	6.1	–	[200]
Nd_2NiO_4	12	56	[204]

stability of Ln_2CuO_4 decreases in the sequence of La → Gd owing to increasing distortions of the crystal lattice with the decreasing REE cation radii [181, 212].

The electrical and magnetic properties of Ln_2CuO_4 have been studied in detail [215–220]. Metallic conductivity is characteristic of lanthanum cuprate in air, whereas the conductivity of the cuprates of other rare-earth elements (Ln = Pr–Gd) is semiconductor-like, reducing with the decreasing REE radii [215, 216]. Doping with divalent metal cations such as Ca, Sr, Ba, or Pb leads regularly to an increase in the conductivity of the cuprates [215, 217, 219, 220]. The TECs of the ceramic $La_{2-x}A_xCuO_4$ (A = Ca, Sr, Ba; $x = 0$–1.0) were calculated from dilatometric data to vary in the range $(11–12) \times 10^{-6}\,K^{-1}$ at 300–470 K and $(12–14) \times 10^{-6}\,K^{-1}$ at 600–900 K [220]. When doping lanthanum cuprate with alkaline-earth cations, a definite degradation in the mechanical properties of the ceramics as well as a decreasing stability in relation to the interaction with water vapor and carbon dioxide contained in atmospheric air were mentioned [220].

A study of the solid solutions of Ln_2CuO_4-Bi_2CuO_4 (Ln = La, Pr, Nd, Sm, Eu, Gd) has been performed [221, 222]. The maximum solid solubility of bismuth in the A sublattice of $Ln_{2-x}Bi_xCuO_4$ corresponds to x values from 0.1 to 0.2, while formation of solid solutions based on bismuth cuprate was stated to be in the range $1.8 \le x \le 2.0$ [221, 222]. Doping by bismuth results in decreasing conductivity and thermal expansion of the $(Ln,Bi)CuO_4$ ceramics [222]. Properties of the individual phase of Bi_2CuO_4 and the $Bi_2(Cu,M)O_4$ (M = Ni, Pd) solid solutions have been reported [81, 223–227].

The present work was not aimed at analysis of the numerous publications on high-temperature superconductors based on cuprates. Researchers interested in such data could be addressed, for example, to a review [228]. Among the results concerning high-temperature electrochemistry, one can list the data on oxygen exchange [229–233] and oxygen permeability of selected superconducting oxides [234–239].

Perovskites ARO_3 (A = Ca, Sr, Ba; R = Zr, Hf, Ce, Ti)

Perovskite-type phases of ARO_3, where A is the alkaline earth element and R = Zr, Hf, or Ce, possess relatively low mixed ionic-electronic conductivity, as a result of which there is little likelihood of the direct use of such oxides in electrochemical cells. However, certain solid solutions based on them exhibit considerable proton conductivity in hydrogen-containing atmospheres. In addition, studying the properties of such oxides may be of interest in developing SOFCs, because the formation of $AZrO_3$-based phases may occur in the diffusion layers between solid electrolytes of stabilized zirconia and perovskite electrodes based on $LnMnO_3$.

Existing perovskite-type phases are characteristic of all the AO–RO_2 (A = Ca, Sr, Ba; R = Zr, Hf, Ce) systems, with the exception of CaO–CeO_2 [240–250]. The thermodynamic stability of the zirconates, $AZrO_3$, increases regularly with the increasing radii of the alkaline earth cations in the sequence Ca < Sr < Ba [251], whereas the stability of barium perovskite compounds was reported to decrease as $BaHfO_3 > BaZrO_3 > BaCeO_3$ [252]. The formation of a continuous series of solid solutions was reported for the $SrZr_{1-x}M_xO_3$ (M = Ce, Hf) systems for $0 \le x \le 1.0$ [253, 254]. For $BaM_{1-x}Y_xO_{3-\delta}$ (M = Zr, Hf, Ce, Th), the concentration range of existing single perovskite phases is close to $0 \le x \le 0.2$ [255]. When doping with copper, solid solutions of $BaM_{1-x-y}Y_xCu_yO_{3-\delta}$ (M = Zr, Hf) were ascertained to form at $0 \le x \le 0.10$ [255].

Most of the perovskites of this group possess mixed ionic-electronic conductivity in air, with electronic conduction provided by electron hole transport [255–257]. In hydrogen-containing atmospheres, the conductivity of numerous ARO_3-based perovskites is predominantly protonic [256–259]. The highest proton conductivity in reducing atmospheres was reported for solid solutions of $BaCe_{0.85}Ln_{0.15}O_{3-\delta}$ with Ln = Nd, Eu, Gd, Dy, Ho, of Lu [258]. The proton conduction in $BaCe_{0.85}Ln_{0.15}O_{3-\delta}$ (Ln = Sc, Sm, La) is somewhat lower, while the ceramics of $BaCe_{0.85}Pr_{0.15}O_{3-\delta}$ exhibit n-type electronic conductivity in reducing environments [258].

For perovskite-like titanates of the alkaline-earth elements, applicability in high-temperature electrochemical devices is considered to be much worse compared to perovskites based on manganites or cobaltites. This is caused by the relatively low ionic and electronic conductivities of the titanates in oxidizing atmospheres (see, for instance, [173–175, 260–263]). One important exception is the $CaTi_{1-x}Fe_xO_{3-\delta}$ solid solutions, which have reasonably high oxygen ionic conductivity in air [262]. One should note also the solid solutions based on the stoichiometric and cation-deficient titanates $LnTiO_3$ (Ln = La, Ce, Pr, Nd) that exhibit high electronic conductivity in reducing atmospheres [2, 264–266], which makes such oxides promising materials for SOFC anodes.

Electrode properties of perovskite oxides in solid electrolyte cells

Electrode materials of high-temperature electrochemical cells should satisfy numerous criteria such as high electronic conductivity, stability under application conditions, a TEC compatible with that of the solid electrolyte, and minimum chemical interaction with other materials of the cell [267–269]. Therefore the properties of electrode layers applied onto solid electrolyte ceramics depend not only on the properties of the electrode material, but also on the method of fabricating the electrochemical cell and on the properties of the electrolyte. This is determined, firstly, by a primary effect of the triple-phase boundary and solid electrolyte surface on the electrochemical processes. Secondly, the

fabrication method and pre-history of the electrode determine its morphology and the activity of its surface. Thirdly, diffusion layers formed due to an interaction between the electrode and the electrolyte materials affect oxygen transport through the electrode/electrolyte interface.

For the perovskite electrodes in contact with zirconia solid electrolytes, the most important influence on the electrochemical activity was demonstrated to be provided by the third factor, i.e. the presence of blocking diffusion layers comprising a pyrochlore phase [270, 271]. In order to avoid formation of the blocking layers, one should minimize both the temperature and the time of sintering the electrode layers deposited onto stabilized zirconia ceramics. Using temperatures for the sintering below 1270 K is preferable [270, 271]. In our research [69, 76, 81, 84–87, 89, 272], sintering aids to the electrode materials were used in order to achieve the minimum temperature and time of sintering of the manganite electrodes, providing coincidentally the necessary mechanical strength of the electrode layers. The maximum electrochemical activity of the electrodes of $(La,Sr)MnO_{3-\delta}$ and $(La,Sr)(Mn,M)O_{3-\delta}$ (M = Ni, Fe) was provided by using sintering additions of bismuth oxide, Bi_2O_3, and bismuth cuprate, Bi_2CuO_4. Creation of cation vacancies in the A sublattice of the lanthanum-strontium manganites leads also to increasing electrochemical activity, which is a result of both suppressing the formation of the blocking layers and increasing the ionic conductivity of the perovskites [89]. Avoidance of incorporating cations of the sintering aid into the A-site vacancies is desirable, and the sintering additions of Bi_2CuO_4 are favored [89]. As substitution of strontium with lead cations also results in a decreasing interaction between the electrode and the electrolyte materials, the overpotential of the $La_{0.6}Pb_{0.4}MnO_{3-\delta}$ electrodes is lower in comparison with that of $La_{0.6}Sr_{0.4}MnO_{3-\delta}$ at equal current densities (Fig. 1).

Using high temperatures of sintering perovskite electrodes on stabilized zirconia ceramics leads to a dramatic increase of the overpotentials. For example, excessively high values of the polarization resistance were obtained for the electrodes of $LnCr_{1-x}Ni_xO_{3-\delta}$ (Ln = La, Sm; x = 0.4–0.8, sintering temperature of 1670 K) [42], $LaCo_{1-x}Ni_xO_{3-\delta}$ (x = 0.3–0.5, sintering temperature of 1570–1620 K) [273], $Ln_{1-x}Ca_xMnO_{3-\delta}$ (x = 0–0.5, sintering temperature of 1700–1750 K) [58, 274], and $La_{0.6}Sr_{0.4}Mn_{1-x}M_xO_{3-\delta}$ (M = Co, Ni; x = 0–0.05, sintering temperature of 1620–1670 K) [82]. Such results, demonstrating an obvious correlation between sintering temperature and overpotential, are of little practical use.

In contrast to the zirconia solid electrolytes, no blocking layers were ascertained to form between perovskite electrodes based on REE cobaltites and Bi_2O_3-based solid electrolytes [115, 142, 158]. This is associated with a sufficiently high ionic conductivity of the complex oxides of the Bi_2O_3–Ln_2O_3–CoO_x systems [142, 275–277]. However, the oxygen transport properties of the intermediate diffusion layers are somewhat worse compared to the Bi_2O_3-based electrolytes, and the electronic conductivity of cobaltites decreases with the incorporation of bismuth cations into their crystal lattice [118, 142, 145, 275]. Therefore, one should reduce the interaction of the materials during fabrication of the electrochemical cells.

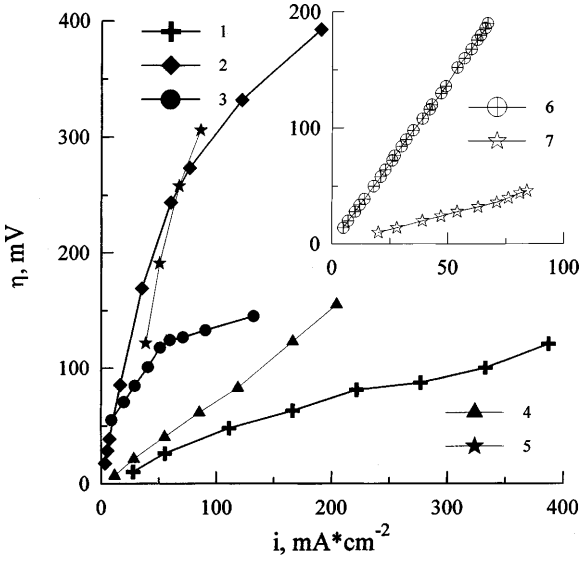

Fig. 1 Dependence of overpotential on current density through perovskite-type electrodes: *1* $La_{0.5}Sr_{0.4}MnO_{3-\delta}$ with sintering aid of Bi_2CuO_4, 1260 K, solid electrolyte of $Zr_{0.90}Y_{0.10}O_{1.95}$ [89]; *2* $La_{0.6}Sr_{0.4}MnO_{3-\delta}$ with sintering aid of Bi_2O_3, 1260 K, solid electrolyte of $Zr_{0.90}Y_{0.10}O_{1.95}$ [89]; *3* $La_{0.6}Pb_{0.4}MnO_{3-\delta}$ with sintering aid of Bi_2O_3, 1245 K, solid electrolyte of $Zr_{0.90}Y_{0.10}O_{1.95}$ [69]; *4* $La_{0.6}Sr_{0.4}Mn_{0.8}Ni_{0.2}O_{3-\delta}$ with sintering aid of Bi_2O_3, 1253 K, $Zr_{0.90}Y_{0.10}O_{1.95}$ [76]; *5* $La_{0.6}Sr_{0.4}Mn_{0.7}Fe_{0.3}O_{3-\delta}$ with sintering aid of Bi_2O_3, 1230 K, $Zr_{0.90}Y_{0.10}O_{1.95}$ [75]; *6* $La_{0.7}Sr_{0.3}CoO_{3-\delta}$, 910 K, solid electrolyte of $Bi_{0.75}Y_{0.25}O_{1.5}$ [95]; *7* $Nd_{0.5}Sr_{0.5}CoO_{3-\delta}$, 910 K, solid electrolyte of $Bi_{0.75}Y_{0.25}O_{1.5}$ [95]. The *curves 1–5* refer to cathodic polarization, whereas the *curves 6* and *7* correspond to anodic polarization. Absolute values of the overpotential are given for convenience

Studying oxide materials of the CeO_2–Gd_2O_3–MO_x (M = Co, Mn) ternary systems leads to the conclusion that there should form no blocking layers between solid electrolytes of doped ceria and electrodes of cobaltites and manganites [96, 278]. In this case, however, it is desirable to minimize interaction of the perovskite electrode and ceria electrolyte materials analogously to the bismuth oxide electrolytes. This is caused by the decrease in oxygen ionic conductivity of gadolinia-doped ceria with additions of the transition metal oxides [96, 278].

Another important factor determining the polarization of the perovskite electrodes refers to the activity of the electrode surface and to the concentration of the active reaction sites near the triple-phase boundary. As an example, electrode layers of $La_{0.7}Sr_{0.3}CoO_{3-\delta}$ sintered onto the zirconia ceramics, even at 1423 K, are desirable to be modified by impregnation with a solution of metal acetates of the same cation composition [271]. Otherwise the polarization resistance of the cobaltite

electrodes was found to be higher by a factor of 10–100, caused by passivation during the sintering and by interaction with the electrolyte, resulting in blocking the triple-phase boundary. The manganite electrodes can be activated either by applying praseodymium oxide and lanthanum-strontium cobaltite onto their surface, or by additions of metallic silver [75, 89, 92]. Figure 2 illustrates the effect of such surface modification on the cathodic overpotential. The activating effect of praseodymium oxide on the electrochemical activity of the manganite electrode layers is determined by the specific catalytic activity of the Pr^{4+} ions in the electrochemical reactions with participating oxygen, being analogous to the influence of praseodymia on the properties of platinum metal electrodes [89, 279]. The higher electrochemical activity of the cobaltite electrodes, related to the activity of the electrodes prepared by sintering cobaltite powders, can be provided by producing electrode layers by spraying metal nitrate solution over heated bismuth oxide electrolyte ceramics [115]. Another promising method to increase the activity of the cobaltite electrodes refers to adding metallic silver into their composition, similar to the electrodes of lanthanum-strontium manganites [141].

The results of studying oxide electrodes in contact with various solid electrolytes show generally an absence of direct correlations between the electrochemical activity of the electrode layers and the oxygen ion transport properties of the corresponding ceramics. Such behavior was observed for electrodes of $(Ln,Sr)CoO_{3-\delta}$ and $Sr(Co,Fe)O_{3-\delta}$ deposited onto δ–Bi_2O_3-based electrolytes [94, 95, 115, 118, 141, 142, 158], and for the manganite electrodes in the zirconia solid electrolyte cells [69, 75, 76, 81, 84–87, 89, 92]. In some cases, an effect of electronic conductivity of the electrode materials on the overpotentials was detected.

Thus, the most important factors determining polarization of the oxide electrodes are as follows: the presence of blocking layers, specific electrocatalytic activity of the electrode, and highly developed electrode morphology. Among the electrode materials exhibiting the best electrochemical properties in contact with bismuth oxide electrolytes, one can mention $Nd_{0.5}Sr_{0.5}CoO_{3-\delta}$ with additions of silver. For cells with electrolytes based on stabilized zirconia, the maximum electrochemical activity was found for $La_{0.5}Sr_{0.4}MnO_{3-\delta}$ with Bi_2CuO_4 as a sintering aid, and $La_{0.6}Sr_{0.4}Mn_{0.8}Ni_{0.2}O_{3-\delta}$ and $La_{0.6}Pb_{0.4}MnO_{3-\delta}$ with additions of Bi_2O_3.

When discussing the properties of the electrode systems, one should separately note the detailed studies of the $La_{0.7}Sr_{0.3}CoO_{3-\delta}$ perovskite electrodes deposited onto the zirconia electrolyte ceramics [229, 270, 271, 280–282]. In particular, the oxygen interphase exchange in such cells was demonstrated by the isotopic method to be primarily determined by the processes at the cobaltite surface. The oxygen exchange rate of the $La_{0.7}Sr_{0.3}CoO_{3-\delta}$ electrodes is close to that of the cobaltite ceramics (Fig. 3). This suggests that the electrode reaction for the cells with zirconia solid electrolytes is localized at the triple-phase boundary and at the oxide electrode surface. In contrast, an active role of the electrolyte surface in electrode reactions can be expected

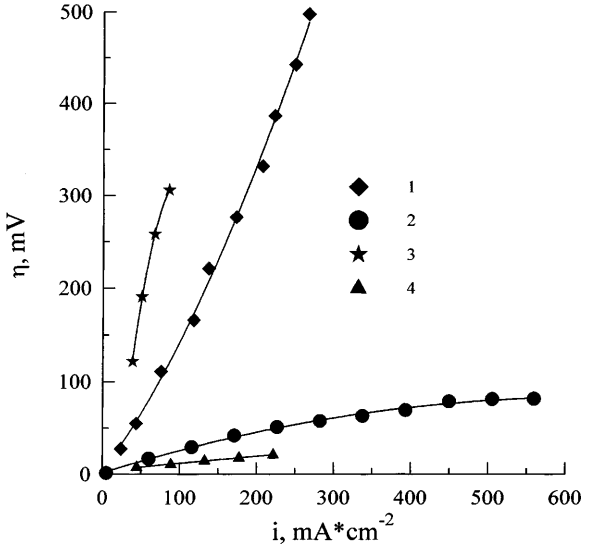

Fig. 2 Dependence of overpotential on cathodic current density for oxide electrodes applied onto $Zr_{0.90}Y_{0.10}O_{1.95}$ solid electrolyte ceramics: *1* $La_{0.5}Sr_{0.4}MnO_{3-\delta}$ with sintering aid of Bi_2CuO_4 at 1225 K, after preparation [89]; *2* the same electrode after activation with praseodymium oxide [89]; *3* $La_{0.6}Sr_{0.4}Mn_{0.7}Fe_{0.3}O_{3-\delta}$ with sintering aid of Bi_2O_3 at 1230 K, after preparation [75]; *4* the same electrode after depositing praseodymium oxide and $La_{0.5}Sr_{0.5}CoO_{3-\delta}$ [75]. Absolute values of the overpotential are given

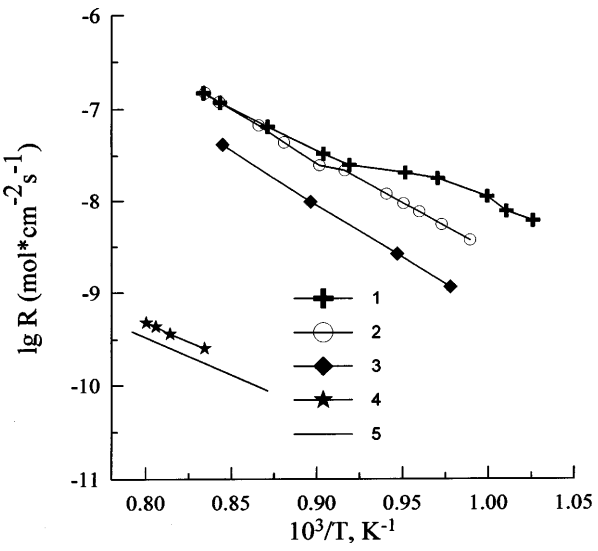

Fig. 3 Temperature dependence of interphase oxygen exchange rate [229, 279, 289]: *1* ceramic $La_{0.7}Sr_{0.3}CoO_{3-\delta}$ (measured by the isotopic exchange method); *2* electrode $La_{0.7}Sr_{0.3}CoO_{3-\delta}$ in contact with $Zr_{0.90}Y_{0.10}O_{1.95}$ solid electrolyte (measured by the isotopic exchange method); *3* electrode $La_{0.7}Sr_{0.3}CoO_{3-\delta}$ in contact with $Zr_{0.90}Y_{0.10}O_{1.95}$ (calculated from the results of measuring overpotential as a function of current density); *4* single crystal of $Zr_{0.90}Y_{0.10}O_{1.95}$; *5* powder of $Zr_{0.90}Y_{0.10}O_{1.95}$

for electrolytes based on bismuth and ceria oxides, both the electronic conductivity and the surface exchange rate of which are much higher in comparison with zirconia [229, 283–286].

References

1. Palguev SF, Gilderman VK, Zemtsov VI (1990) High-temperature oxide electronic conductors for electrochemical devices (in Russian). Nauka, Moscow
2. Bazuev GV, Shveikin GP (1985) Complex oxides of elements with completing d- and f-shells (in Russian). Nauka, Moscow
3. Pavlikov VN, Shevchenko AV, Lopato LM, Tresvyatsky SG (1967) Chromites of rare-earth elements and their physicochemical properties. In: Chemistry of high-temperature materials (in Russian). Nauka, Moscow
4. Tresvyatsky SG, Pavlikov VN (1964) Problems of theory and applications of rare-earth metals (in Russian). Nauka, Moscow, pp 159–162
5. Tresvyatsky SG, Lopato LM, Pavlikov VN, Shevchenko AV (1968) Rev Int Hautes Temp Refract 5: 45
6. Portnoy KI, Mordovin OA, Timofeeva NI (1968) Neorg Mater 4: 1368
7. Shevchenko AV, Lopato LM, Tresvyatsky SG (1966) Neorg Mater 2: 1240
8. Portnoy KI, Timofeeva NI (1965) Neorg Mater 1: 1593
9. Shevchenko AV, Lopato LM, Pavlikov VN (1969) Neorg Mater 5: 2128
10. Tresvyatsky SG, Pavlikov VN, Lopato LM (1966) Neorg Mater 2: 269
11. Lopato LM (1972) PhD Thesis, Institute of Materials Science Problems, Ukrainian Academy of Sciences
12. Petrov AN, Kropanev AYu, Zhukovsky VM, Cherepanov VA, Neudachina GK (1981) Zh Neorg Khim 26: 3190
13. Kropanev AYu, Petrov AN (1983) Neorg Mater 19: 2027
14. Pavlikov VN, Shevchenko AV, Lopato LM, Tresvyatsky SG (1966) Neorg Mater 2: 679
15. Tolochko SP, Kononyuk IF, Zonov YuG, Ivashkevich LS (1987) Neorg Mater 23: 829
16. Andrianov MA, Balkevich VP, Sotnikov VE (1980) Ogneupory (11): 42
17. Tolochko SP, Kononyuk IF, Ivashkevich LS (1987) Neorg Mater 23: 1892
18. Anikina EL, Zemtsov VI, Burmakin EI, Antonov BD (1994) Neorg Mater 30: 1060
19. Anikina EL, Zemtsov VI, Gorelov VP, Burmakin EI (1996) Neorg Mater 32: 364
20. Rubinchik YaS, Pavlyuchenko MM, Mochalnik IA (1969) Vesti Akad Nauk BSSR Ser Khim (2): 23
21. Savchenko VF, Rubinchik YaS (1979) Neorg Mater 15: 122
22. Savchenko VF, Rubinchik YaS (1976) Vesti Akad Nauk BSSR Ser Khim (2): 53
23. Savchenko VF, Rubinchik YaS (1972) Vesti Akad Nauk BSSR Ser Khim (3): 75
24. Savchenko VF, Rubinchik YaS, Pavlyuchenko MM (1973) Vesti Akad Nauk BSSR Ser Khim (5): 87
25. Savchenko VF, Rubinchik YaS (1976) Vesti Akad Nauk BSSR Ser Khim (5): 41
26. Rubinchik YaS, Veremey TP, Pavlyuchenko MM, Mochalnik IA (1973) Dokl Akad Nauk BSSR 17: 830
27. Shvaiko-Shvaikovsky VE, Popov VP, Gordon VG (1979) Neorg Mater 15: 1441
28. Rubinchik YaS, Reznikov MYa (1973) Dokl Akad Nauk BSSR 17: 434
29. Spitsyn VM, Pitov VA, Kolesnikov AK, Kuznetsov DG, Sulonitsky YuL, Spiridonov FN (1981) Dokl Akad Nauk SSSR 258: 1377
30. Bliznyuk VA, Donzova TK, Kiyamsky BD (1980) USSR Patent 710951
31. Zemtsov VI (1985) PhD Thesis, Ural State University, Sverdlovsk
32. Zaitseva ZA, Litvin AL (1979) Dokl Akad Nauk SSSR Geol Khim Biol Nauki (1): 27
33. Dzhaoshvili KR, Baratashvili IB, Omiadze IS, Popov SG, Nadiradze AA (1989) Zh Prikl Khim 62: 254
34. Gilderman VK, Zemtsov VI, Palguev SF (1987) Neorg Mater 23: 1001
35. Gordon VG, Rekov AI, Spiridonov EG, Timofeeva NI (1971) Neorg Mater 7: 1084
36. Zhuk PP, Vecher AA, Mobius H-H, Samokhval VV (1987) Vestn Belarus Univ Ser 2 (1): 5
37. Kononyuk IF, Tolochko SP, Surmach NG (1986) Neorg Mater 22: 98
38. Tolochko SP, Kononyuk IF (1986) Neorg Mater 22: 1696
39. Zhuk PP, Vecher AA, Samokhval VV, Naumovich EN, Viskup AP (1988) Neorg Mater 24: 105
40. Palguev SF, Zemtsov VI, Gilderman VK, Neuimin AD (1984) Solid State Ionics 13: 65
41. Palguev SF, Gilderman VK, Zemtsov VI (1987) Int Ceram 13: 119
42. Ivanova NP, Sonin VI, Zharsky IM (1990) Elektrokhimiya 26: 105
43. Zemtsov VI, Gilderman VK, Palguev SF (1988) Neorg Mater 24: 1865
44. Zhuk PP, Vecher AA, Samokhval VV, Mobius H-H (1985) Vestn Belarus Univ Ser 2 (1): 5
45. Grigor'eva NV, Reznikova ED, Spiridonov EG (1980) Neorg Mater 16: 2020
46. Nedilko SA, Panchenko GV (1987) Ukrain Khim Zh 53: 457
47. Tolochko SP, Kononyuk IF, Lyutsko VA, Zonov YuG (1987) Neorg Mater 23: 1520
48. Nedilko SA, Panchenko GV (1989) Ukrain Khim Zh 55: 462
49. Gorbachev VV, Kvaskov VB (1978) Neorg Mater 14: 1855
50. Golub AM, Nedilko SA, Gozhdzinsky SM (1978) Neorg Mater 14: 1859
51. Tolochko SP (1987) PhD Thesis, Belarus State University, Minsk
52. Kharton VV, Kovalevsky AV, Tikhonovich VN, Naumovich EN, Viskup AP (1998) Solid State Ionics 110: 53
53. Nedilko SA, Sidorik LS, Gozhdzinsky SM (1979) Vestn Kiev Univ Khim (19): 21
54. Nedilko SA, Panchenko GV, Nadkrinichnaya AP (1989) Vestn Kiev Univ Khim (30): 41
55. Shirvinskaya AK, Petrova MA (1987) Phase diagrams of high-melting oxide systems. A handbook, vol. 5, part 3 (in Russian). Nauka, Leningrad
56. Shaplygin IS, Kakhan BG, Lazarev VB (1979) Zh Neorg Khim 24: 1478
57. Shaplygin IS, Lazarev VB (1985) Zh Neorg Khim 30: 1595
58. Tikhonova LA (1991) PhD Thesis, Belarus State University, Minsk
59. Nedilko SA, Polischuk VV, Zyryanova NP (1980) Ukrain Khim Zh 46: 1137
60. Rubinchik YaS, Prokudina SA, Pavlyuchenko MM (1973) Neorg Mater 9: 1951
61. Vorob'ev YuP, Iovlev AA, Leontyev SA, Men AN, Prokudina SA, Rubinchik YaS (1979) Neorg Mater 15: 1449
62. Rubinchik YaS, Prokudina SA (1979) Vesti Akad Nauk BSSR Ser Khim (4): 70
63. Tikhonova LA, Vecher AA, Samal GI, Zhuk PP, Tonoyan AA, Gilevich MP (1988) Vestn Belorus Univ Ser 2 (3): 13
64. Tikhonova LA, Samal GI, Zhuk PP, Tonoyan AA, Vecher AA (1990) Neorg Mater 26: 184
65. Tikhonova LA, Zhuk PP, Vecher AA, Gilevich MP, Samal GI (1990) Neorg Mater 26: 2580
66. Tikhonova LA, Zhuk PP, Tonoyan AA, Vecher AA (1991) Neorg Mater 27: 360
67. Tikhonova LA, Zhuk PP, Zinkevich MV, Vecher AA (1990) Vesti Akad Nauk BSSR Ser Khim (5): 42
68. Podsekin AK, Demyanov VV, Ivanova VV, Venevtsev YuV (1976) Neorg Mater 12: 2192

69. Gaiduk YuS, Kharton VV, Naumovich EN, Nikolaev AV, Samokhval VV (1994) Inorg Mater 30: 1360
70. Bogdanovich NM, Khomyakova NG, Maizner EA (1993) Synthesis and sintering of lanthanum-strontium manganites. In: Perfilyev MV (ed) Ionics of solid state (in Russian). Nauka, Ekaterinburg, pp 54–64
71. Pavlov VI, Bogush AK, Bychkov GL (1984) Neorg Mater 20: 863
72. Pavlov VI, Bychkov GL, Bogush AK (1982) Investigation of crystal structure of $(La_{1-x}Me_x)MnO_3$ (Me^{2+} = Ca, Ba,Sr,Cd,Pb). In: Physical properties of gases and solids (in Russian). Minsk State Pedagogical Institute, Minsk, pp 52–59
73. Zhuk PP, Samokhval VV, Vecher AA (1985) Vestn Belorus Univ Ser 2 (1): 3
74. Zhuk PP, Vecher AA, Samokhval VV (1986) Neorg Mater 22: 522
75. Tikhonovich VN, Kharton VV, Naumovich EN (1997) Inorg Mater 33: 718
76. Gaiduk YuS, Kharton VV, Naumovich EN, Samokhval VV (1994) Inorg Mater 30: 759
77. Korolev VP, Kononyuk IF (1986) Vestn Belorus Univ Ser 2 (3): 13
78. Korolev VP, Kononyuk IF, Popov IO (1989) Neorg Mater 25: 1192
79. Tikhonova LA, Zhuk PP, Vecher AA (1993) Influence of doping with alkaline-earth metals on physical-chemical properties of rare-earth manganites. In: Perfilyev MV (ed) Ionics of solid state (in Russian). Nauka, Ekaterinburg, pp 14–25
80. Kononyuk IF, Zakharov VI, Khramelya TV, Gindin EI (1991) Neorg Mater 27: 1915
81. Kharton VV, Nikolaev AV, Naumovich EN, Vecher AA (1995) Solid State Ionics 81: 201
82. Tikhonova LA, Zhuk PP, Poluyan AF, Alfer SA, Vecher AA (1997) Elektrokhimiya 33: 1332
83. Kozhevnikova TR, Bogdanovich NM, Neuimin AD, Zhuravlev BV (1993) Influence of copper (I) oxide additions on electrical conductivity of lanthanum-strontium manganites. In: Perfilyev MV (ed) Ionics of solid state (in Russian). Nauka, Ekaterinburg, pp 65–69
84. Naumovich EN, Kharton VV, Vecher AA, Nikolaev AV, Abugoffa AA (1995) Properties of solid solutions based on $LaMnO_3$. In: Dokiya M, Tagawa H, Yamamoto O, Singhal SC (eds) Solid oxide fuel cells IV. Electrochemical Society, Pennington, NJ, pp 520–527
85. Kharton VV, Naumovich EN, Vecher AA, Nikolaev AV (1994) Materials for solid oxide fuel cells. In: Filimov VA (ed) Proc int symp on cold fusion and advanced energy sources (in Russian). SIEM Minsk, Belarus, pp 113–117
86. Nikolaev AV, Kharton VV, Naumovich EN, Vecher AA (1994) SOFC cathode materials. In: Bossel U (ed) Proc 1st European SOFC forum, vol 1. Lucerne, Switzerland, pp 415–424
87. Kharton VV, Naumovich EN, Vecher AA, Nikolaev AV (1995) Materials of SOFC cathode. In: Savadogo O, Roberge P, Veziroglu T (eds) Proc 1st int symp on new materials for fuel cell systems. Montreal, Canada, pp 512–520
88. Arzhannikov VA (1985) PhD Thesis, Ural Dept of the Academy of Sciences of USSR, Sverdlovsk
89. Tikhonovich VN, Kharton VV, Naumovich EN, Savitsky AA (1998) Solid State Ionics 106: 197
90. Kharton VV, Viskup AP, Naumovich EN, Tonoyan AA, Reut OP (1998) Mater Res Bull 33: 1087
91. Lyubkina IYa, Kononyuk IF (1986) Neorg Mater 22: 979
92. Kharton VV, Naumovich EN, Tikhonovich VN, Vecher AA, Samokhval VV (1996) Vestn Belorus Univ Ser 2 (1): 3
93. Pavlotsky YaV, Loginova MV, Polyansky AV, Sheftel IT (1977) Neorg Mater 13: 485
94. Naumovich EN (1991) PhD Thesis, Belarus State University, Minsk
95. Kharton VV, Naumovich EN (1993) Russ J Electrochem 29: 1297
96. Naumovich EN, Kharton VV, Kovalevsky AV, Samokhval VV (1996) Conjugate transport of oxygen ions and electrons in fluorite-type ceramics $Ce(Gd,M)O_2$ (M = Co, Mn). In: Poulsen F, Bananos N, Linderoth S, Mogensen M, Zachau-Christiansen B (eds) High temperature electrochemistry: ceramics and metals. Roskilde, Denmark, pp 375–380
97. Kharton VV, Naumovich EN, Nikolaev AV (1996) J Membr Sci 111: 149
98. Samokhval VV, Kharton VV, Naumovich EN, Vecher AA (1994) Methods to investigate charge particles transport in oxide materials. Textbook for students (in Russian). Belarus State University, Minsk
99. Petrov AN, Lipatov NI, Zybin DN, Rabinovich LYa, Kononchuk OF (1988) Neorg Mater 24: 294
100. Kononchuk OF, Petrov AN, Cherepanov VA (1991) Neorg Mater 27: 1963
101. Kononchuk OF (1991) PhD Thesis, Ural State University, Sverdlovsk
102. Kropanev AYu (1981) PhD Thesis, Ural State University, Sverdlovsk
103. Petrov AN, Kropanev AYu, Zhukovsky VM (1984) Zh Fiz Khim 58: 50
104. Kropanev AYu, Petrov AN, Zhukovsky VM (1983) Zh Neorg Khim 28: 2938
105. Cherepanov VA, Petrov AN, Grimova LYu (1985) Zh Fiz Khim 59: 2131
106. Cherepanov VA, Barkhatova LYu, Petrov AN, Voronin VI (1995) Phase equilibria in the La-Sr-Co-O system and thermodynamic stability of the single phases. In: Dokiya M, Tagawa H, Yamamoto O, Singhal SC (eds) Solid oxide fuel cells IV. Electrochemical Society, Pennington, NJ, pp 434–443
107. Grimova LYu, Cherepanov VA, Petrov AN (1987) Thermodynamic stability boundaries of $La_{1-x}Sr_xCoO_3$ ($0.1 \le x \le 0.3$) solid solutions. In: Proc 4th Sov conf on physics and chemistry of rare-earth semiconductors (in Russian). Novosibirsk, p 105
108. Petrov AN, Cherepanov VA, Zuev AYu (1987) Zh Fiz Khim 61: 630
109. Glazyrina VI (1991) PhD Thesis, Ural State University, Sverdlovsk
110. Kniga MV, Vygovsky II, Klementovich EE (1979) Zh Neorg Khim 24: 1171
111. Petrov AN (1987) Some problems of thermodynamics and kinetics of solid-state synthesis of $LnCoO_3$ (Ln – lanthanide). In: Proc 4th Sov conf on physics and chemistry of rare-earth semiconductors (in Russian). Novosibirsk, p 103
112. Kropanev AYu, Petrov AN, Rabinovich LYa (1984) Neorg Mater 20: 139
113. Petrov AN, Rabinovich LYa, Zhukovsky VM, Zhukovskaya AS (1987) Dokl Akad Nauk SSSR 292: 372
114. Ostroushko AA, Zhuravleva LI, Kononchuk OF, Petrov AN (1991) Zh Neorg Khim 36: 6
115. Kharton VV (1993) PhD Thesis, Belorus State University, Minsk
116. Kharton VV, Naumovich EN, Nikolaev AV, Vecher AA (1993) Vesti Akad Nauk Belarusi Ser Khim (3): 53
117. Kharton VV, Naumovich EN, Vecher AA, Nikolaev AV (1995) J Solid State Chem 120: 128
118. Kharton VV, Naumovich EN, Zhuk PP, Demin AK, Nikolaev AV (1992) Sov J Electrochem 28: 1376
119. Kharton VV, Naumovich EN, Vecher AA, Nikolaev AV (1995) SOFC cathode material based on rare earth cobalties. In: Dokiya M, Tagawa H, Yamamoto O, Singhal SC (eds) Solid oxide fuel cells IV. Electrochemical Society, Pennington, NJ, pp 512–519
120. Shuk P, Kharton V, Samochval V (1991) Mater Sci Forum 76: 161
121. Kharton VV, Zhuk PP, Demin AK, Nikolaev AV, Tonoyan AA, Vecher AA (1993) Physicochemical properties of $Ln_{1-x}Sr_xCoO_3$ (Ln = La, Pr, Nd, Sm, Gd). In: Perfilyev MV (ed) Ionics of solid state (in Russian). Nauka, Ekaterinburg, pp 3–13
122. Cherepanov VA, Petrov AN, Kropanev AYu, Gorchakova OV, Zhukovsky VM (1981) Zh Fiz Khim 55: 1856

123. Tolochko SP, Kononyuk IF, Makhnach LV (1981) Neorg Mater 17: 1031
124. Vashuk VV, Kononyuk IF, Zonov YuG, Golovchan ON (1992) Neorg Mater 28: 637
125. Kharton VV, Demin AK (1993) Inorg Mater 29: 287
126. Kharton VV, Zhuk PP, Tonoyan AA, Vecher AA (1990) Vesti Akad Nauk BSSR Ser Khim (6): 50
127. Kharton VV, Zhuk PP, Tonoyan AA, Samokhval VV, Vecher AA (1991) Vesti Akad Nauk BSSR Ser Khim (1): 37
128. Kharton VV, Zhuk PP, Tonoyan AA, Vecher AA (1991) Vesti Akad Nauk BSSR Ser Khim (3): 35
129. Zhuk PP, Kharton VV, Tonoyan AA, Naumovich EN (1991) Neorg Mater 27: 1294
130. Kharton VV, Zhuk PP, Vecher AA, Tonoyan AA (1990) Vestn Belorus Univ Ser 2 (2): 8
131. Petrov AN, Kononchuk OF, Andreev AV, Cherepanov VA, Kofstad P (1995) Solid State Ionics 80: 189
132. Kharton VV, Naumovich EN, Nikolaev AV, Samokhval VV (1996) Development of mixed conductive materials for high-temperature electrochemical oxygen membranes. In: Poulsen F, Bananos N, Linderoth S, Mogensen M, Zachau-Christiansen B (eds) High temperature electrochemistry: ceramics and metals. RISQ National Laboratory, Roskilde, Denmark, pp 301–306
133. Kharton VV, Naumovich EN, Kovalevsky AV, Viskup AP, Yaremchenko AA, Bashmakov IA (1998) Solid State Ionics (in press)
134. Kharton VV, Zhuk PP, Tonoyan AA, Zhabko TE, Vecher AA (1991) Inorg Mater 27: 2240
135. Kharton VV, Viskup AP, Bochkov DM, Naumovich EN, Reut OP (1998) Solid State Ionics 110: 61
136. Yaremchenko AA, Kharton VV, Naumovich EN, Klavsut GN, Samokhval VV (1999) Vesti Akad Nauk Belarusi Ser Khim 1:77
137. Kharton VV, Viskup AP, Naumovich EN, Lapchuk NM (1997) Solid State Ionics 104: 67
138. Yaremchenko AA, Kharton VV, Viskup AP, Naumovich EN, Tikhonovich VN, Lapchuk NM (1999) Solid State Ionics (in press)
139. Tolochko SP, Kononyuk IF, Makhnach LV (1983) Vestn Belorus Univ Ser 2 (1): 6
140. Shuk P, Vecher A, Kharton V, Tichonova L, Wiemhoefer H-D, Goepel W (1993) Sens Actuators B 15–16: 401
141. Naumovich EN, Kharton VV, Samokhval VV, Kovalevsky AV (1997) Solid State Ionics 93: 95
142. Kharton VV, Naumovich EN, Samokhval VV (1997) Solid State Ionics 99: 269
143. Tolochko SP, Kononyuk IF, Lamekina LM (1983) Zh Neorg Khim 28: 1396
144. Kharton VV, Zhuk PP, Vecher AA, Astashko VV, Gurlo ACh (1992) Vestn Belorus Univ Ser 2 (1): 19
145. Zhuk PP, Zinkevich MV, Kharton VV, Vecher AA (1991) Vestn Belorus Univ Ser 2 (2): 18
146. Petrov AN, Kononchuk OF, Andreev AV, Cherepanov VA, Kofstad P (1995) Solid State Ionics 80: 189
147. Barkhatova LYu, Klimenko AI, Kononchuk OF, Petrov AN, Sergeev SV (1990) Zh Fiz Khim 64: 3098
148. Kovalevsky AV, Kharton VV, Tikhonovich VN, Naumovich EN, Tonoyan AA, Reut OP, Boginsky LS (1998) Mater Sci Eng B 52: 105
149. Kharton VV, Naumovich EN, Nikolaev AV (1996) Solid State Ionics 83: 301
150. Mobius H-H (1986) Oxygen current density coefficient of oxidic materials as a parameter for selection in development of elecrodes with solid electrolytes. In: Extend abstr 37th meet ISE, vol 1. VINITI, Lubertsi, pp 136–139
151. Kononyuk IF, Tolochko SP, Surmach NG, Nikitina TP, Tarnovetsky IM (1987) Zh Neorg Khim 32: 2789
152. Pavlotsky YaV, Ulyanova TP, Budim NI, Rubalsky GD, Gindin EI (1986) Neorg Mater 22: 131
153. Pavlotsky YaV, Ulyanova TP, Bondarenko EG, Budim NI (1989) Neorg Mater 25: 1400
154. Svirina EP, Shlyakhina LP, Lukina MM, Ntakhomvukiye V (1986) Fiz Tverd Tela 28: 1898
155. Kononyuk IF, Surmach NG, Tolochko SP, Kugan TV (1984) Neorg Mater 28: 1203
156. Yaremchenko AA, Kharton VV, Viskup AP, Naumovich EN, Lapchuk NM, Tikhonovich VN (1998) J Solid State Chem 142: 325
157. Kharton VV, Viskup AP, Naumovich EN, Tikhonovich VN (1999) Mater Res Bull (in press)
158. Kharton VV, Naumovich EN, Nikolaev AV, Astashko VV, Vecher AA (1993) Russ J Electrochem 29: 1039
159. Vashuk VV, Prodan AS, Zinkevich MV, Olshevskaya OP (1993) Neorg Mater 29: 641
160. Vashook VV, Zinkevich MV, Ulmann H, Teske K (1996) Oxygen diffusion in the non-stoichiometric perovskite strontium cobalt oxide. In: Poulsen F, Bananos N, Linderoth S, Mogensen M, Zachau-Christiansen B (eds) High temperature electrochemistry: ceramics and metals. RISQ National Laboratory, Roskilde, Denmark, pp 467–472
161. Kharton VV, Nikolaev AV, Naumovich EN, Samochval VV (1994) Inorg Mater 30: 492
162. Zinkevich MV, Vashuk VV (1992) Neorg Mater 28: 816
163. Kharton VV, Skilkov SA, Nikolaev AV, Naumovich EN, Leonidov IA, Patrikeev MV, Samokhval VV (1994) Inorg Mater 30: 896
164. Zinkevich MV, Vashuk VV (1993) Vesti Akad Nauk Belarusi Ser Khim (3): 48
165. Zinkevich MV, Vashuk VV (1992) Elektrokhimiya 28: 1800
166. Kharton VV, Zhuk PP, Demin AK, Nikolaev AV, Tonoyan AA, Vecher AA (1992) Inorg Mater 28: 1406
167. Kharton VV, Naumovich EN (1993) Dokl Akad Nauk Belarusi 37: 57
168. Kharton VV, Astashko VV, Zhuk PP, Demin AK, Nikolaev AV, Gilevich MP, Vecher AA (1992) Vesti Akad Nauk Belarusi Ser Khim (1): 47
169. Kharton VV, Astashko VV, Zhuk PP, Demin AK, Tonoyan AA, Gilevich MP, Vecher AA (1992) Vesti Akad Nauk Belarusi Ser Khim (3/4): 70
170. Kharton VV, Naumovich EN, Nikolaev AV (1994) Solid State Phenom 39–40: 147
171. Kovalevsky AV, Kharton VV, Naumovich EN (1997) Elektrokhimiya 33: 184
172. Naumovich EN, Kharton VV, Nikolaev AV, Vecher AA (1995) Properties of solid solutions $SrCo_{1-x}M_xO_3$ (M = Cr..Cu, x = 0..0.5). In: Savadogo O, Roberge P, Veziroglu T (eds) Proc 1st int symp on new materials for fuel cell systems. Montreal, Canada, pp 491–499
173. Kharton VV, Shuangbao Li, Kovalevsky AV, Naumovich EN (1997) Solid State Ionics 96: 141
174. Kharton VV, Shuangbao Li, Kovalevsky AV, Viskup AP, Naumovich EN, Tonoyan AA (1998) Mater Chem Phys 53: 6
175. Kovalevsky AV, Kharton VV, Shuangbao Li, Naumovich EN (1996) Oxygen ion transport in $SrTi(Co)O_{3-\delta}$ perovskites. In: Baptista JL, Labrincha JA, Vilarinho PM (eds) Proc Int Conf Electroceramics-V. Aveiro, Portugal, pp 199–202
176. Kharton VV, Tikhonovich VN, Shuangbao Li, Naumovich EN, Kovalevsky AV, Viskup AP, Bashmakov IA, Yaremchenko AA (1998) J Electrochem Soc 145: 1363
177. Kharton VV, Kovalevsky AV, Viskup AP, Naumovich EN, Reut OP (1998) Oxygen permeation through perovskite-like $SrCo(M)O_{3-\delta}$ (M = Ti, V, Cr, Fe, Cu) and $Sr(Ln)CoO_{3-\delta}$ (Ln = La, Nd, Sm, Gd). In: Ramanarayanan TA (ed) Ionic and mixed conducting ceramics III. Electrochemical Society, Pennington, NJ, pp 736–750
178. Kharton VV, Naumovich EN, Kovalevsky AV, Yaremchenko AA, Viskup AP, Kerko PF, Tikhonovich VN (1999) J Membr Sci (in press)
179. Petrov AN, Zuev AYu, Cherepanov VA, Kropanev AYu, Khrustov VR (1987) Neorg Mater 23: 949
180. Petrov AN, Zuev AYu, Cherepanov VA, Kononchuk OF (1987) Neorg Mater 23: 1044

181. Petrov AN, Zuev AYu, Cherepanov VA (1988) Zh Fiz Khim 62: 3092
182. Tretyakov YuD, Kaul AR, Makukhin NV (1976) J Solid State Chem 17: 183
183. Cherepanov VA, Petrov AN, Grimova LYu, Novitsky EM (1983) Zh Fiz Khim 57: 859
184. Golub AM, Sidorik LS, Nedilko SA, Fedoruk TP (1978) Neorg Mater 14: 1866
185. Kononyuk IF, Makhnach LV, Surmach NG, Vashuk VV, Lyashevich AS (1982) Neorg Mater 18: 429
186. Nedilko SA, Vasyagina RD, Sidorik LS, Ermakova MN, Gozhdzinsky SM (1980) Ukr Khim Zh 46: 251
187. Savchenko VF (1981) Neorg Mater 17: 1654
188. Savchenko VF, Lyubkina IYa (1986) Neorg Mater 22: 1483
189. Savchenko VF, Ivashkevich LS, Lyubkina IYa (1988) Zh Neorg Khim 33: 30
190. Tkalich AK, Glazkov VP, Somenkov VA, Shilshtein SSh, Karkin AE, Mirmelshtein AV (1991) Sverkhprovodimost Fiz Khim Tekhn 4: 2380
191. Timofeeva NI, Romanovich IV (1971) Neorg Mater 7: 2104
192. Kniga MV, Zaretskaya RA (1971) Neorg Mater 7: 464
193. Brach BYa, Melnik GI, Chezhina NV (1973) Vestn Leningrad Univ (16): 143
194. Makhnach LV, Kononyuk IF (1986) Neorg Mater 22: 1687
195. Makhnach LV, Kononyuk IF (1988) Neorg Mater 24: 1348
196. Bochkov DM, Kharton VV, Kovalevsky AV, Viskup AP, Naumovich EN (1999) Solid State Ionics (in press)
197. Vashuk VV, Zinkevich MV, Makhnach LV, Tolochko SP, Kononyuk IF (1998) Neorg Mater 34: 622
198. Tolochko SP, Kononyuk IF, Novik SF (1985) Zh Neorg Khim 30: 2079
199. Kononyuk IF, Surmach NG, Makhnach LV (1982) Neorg Mater 18: 1222
200. Tolochko SP, Kononyuk IF, Strelchik SF, Korzyuk EA (1984) Vesti Akad Nauk BSSR Ser Khim (4): 67
201. Makhnach LV, Tolochko SP, Kononyuk IF, Vashuk VV, Prodan SA (1993) Neorg Mater 29: 1678
202. Tolochko SP, Makhnach LV, Kononyuk IF, Vashuk VV (1994) Zh Neorg Khim 39: 1092
203. Makhnach LV, Kononyuk IF, Tolochko SP (1988) Vesti Akad Nauk BSSR Ser Khim (5): 47
204. Kononyuk IF, Tikhonova LA, Makhnach LV (1981) Neorg Mater 17: 161
205. Brach BYa, Ryabkov YuI, Chezhina NV (1985) Vestn Leningrad Univ (25): 90
206. Vashuk VV, Olshevskaya OP, Prodan SA, Zonov YuG, Tolochko SP (1994) Neorg Mater 30: 972
207. Vashuk VV, Olshevskaya OP, Savchenko VF, Puchkaeva EYa (1994) Neorg Mater 30: 1454
208. Vashuk VV, Olshevskaya OP, Prodan SA (1996) Neorg Mater 32: 488
209. Tretyakov YuD, Kaul AR, Makukhin NV (1976) J Solid State Chem 17: 183
210. Kaul AR (1973) PhD Thesis, Moscow State University, Moscow
211. Nedilko SA (1982) Zh Neorg Khim 27: 1130
212. Lazarev VB, Shaplygin IS (1981) Zh Neorg Khim 26: 1755
213. Shaplygin IS, Porotnikov NV (1984) Zh Neorg Khim 29: 853
214. Nedilko SA, Ermakova SA, Zyryanova NP, Vasyagina RD, Krasilnikova SG (1980) Neorg Mater 16: 1123
215. Shaplygin IS, Kakhan BG, Lazarev VB (1979) Zh Neorg Khim 24: 1478
216. Konovalova IA, Lazarev VB, Morozova EB, Shaplygin IS (1980) Zh Neorg Khim 25: 910
217. Tikhonova LA, Kononyuk IF, Makhnach LV, Zhavnerko GK (1982) Vestn Belorus Univ Ser 2 (2): 15
218. Andreev AV, Petrov AN, Naysh VE, Zuev AYu, Verkhovsky SV (1987) Fiz Met Metalloved 64: 378
219. Mikhaylov IG, Moiseev DP, Toplygo SK, Uvarova SK (1987) Fiz Nizk Temp 13: 985
220. Kononyuk IF, Tikhonova LA, Makhnach LV, Zhavnerko GK (1983) Neorg Mater 19: 934
221. Nedilko SA, Zyryanova NP, Panchenko GV (1986) Ukr Khim Zh 52: 356
222. Tikhonova LA, Kononyuk IF, Zonov YuG, Makhnach LV (1990) Neorg Mater 26: 1495
223. Kargin YuF, Skorikov VM (1989) Zh Neorg Khim 34: 2713
224. Kakhan BG, Lazarev VB, Shaplygin IS (1979) Zh Neorg Khim 24: 1663
225. Poluyan AF (1987) PhD Thesis, Belarus State University, Minsk
226. Kakhan BG, Lazarev VB, Shaplygin IS, Ellert OG (1981) Zh Neorg Khim 26: 232
227. Tikhonovich VN, Bochkov DM, Kharton VV, Naumovich EN, Viskup AP (1998) Mater Res Bull 33: 89
228. Golovashkin AI (1987) Usp Fiz Nauk 152: 553
229. Kurumchin EKh (1997) DSc Thesis, Institute of High-Temperature Electrochemistry RAS, Ekaterinburg
230. Kurumchin EKh, Vdovin GK, Fotiev AA, Leonidova ON (1993) Sverkhprovodimost Fiz Khim Tekhn 6: 1926
231. Kurumchin EKh, Vdovin GK, Photiev AA, Leonidova ON (1994) Solid State Ionics 70/71: 77
232. Kurumchin EKh, Tsidilkovskii VI, Ezin AN, Vdovin GK, Leonidov IA (1994) Sverkhprovodimost Fiz Khim Tekhn 7: 1065
233. Vashuk VV, Golovchan ON, Kononyuk IF, Makhnach LV, Shalaeva TN (1989) Vesti Akad Nauk BSSR Ser Khim (2): 27
234. Patrakeev MV (1996) PhD Thesis, Institute of Solid State Chemistry, Ural Dept of RAS, Ekaterinburg
235. Patrakeev MV, Leonidov IA, Kozhevnikov VL, Tsidilkovskii VI, Demin AK, Nikolaev AV (1993) Solid State Ionics 66: 61
236. Patrakeev MV, Leonidov IA, Kozhevnikov VL, Tsidilkovskii VI, Demin AK (1993) Physica C210: 213
237. Patrakeev MV, Leonidov IA, Kozhevnikov VL, Tsidilkovskii VI, Demin AK, Nikolaev AV (1992) Sverkhprovodimost Fiz Khim Tekhn 5: 1912
238. Patrakeev MV, Leonidov IA, Kozhevnikov VL, Demin AK (1994) Elektrokhimiya 30: 1470
239. Patrakeev MV, Leonidov IA, Kozhevnikov VL (1995) Solid State Ionics 82: 5
240. Toropov NA, Barzakovskii VP, Lapin VV, Kurtseva NN (1969) Phase diagrams of silicate systems. A handbook, vol 1 (in Russian). Nauka, Leningrad
241. Godina NA, Keler EK (1961) Ogneupory 26: 426
242. Kachalova AP, Avgustinnik AI (1959) Zh Prikl Khim 32: 1451
243. Tarnopolskaya RA, Gulko NV (1966) Dokl Akad Nauk SSSR 170: 1140
244. Galkin YuM, Chukhlantsev VG (1965) Neorg Mater 1: 1952
245. Keler EK, Kuznetsov AK (1961) Zh Prikl Khim 34: 2146
246. Godina NA, Keler EK (1959) Zh Neorg Khim 4: 884
247. Keler EK, Godina NA, Kalinina AM (1957) Zh Neorg Khim 2: 209
248. Keler EK, Godina NA, Kalinina AM (1956) Zh Neorg Khim 1: 2556
249. Kravchinskaya MV (1985) Zirconate systems. In: Galakhov FYa (ed) Phase diagrams of high-melting oxide systems. A handbook, vol 5, part 1 (in Russian). Nauka, Leningrad, pp 303–338
250. Kravchinskaya MV (1985) Hafnate systems. In: Galakhov FYa (ed) Phase diagrams of high-melting oxide systems. A handbook, vol 5, part 1 (in Russian). Nauka, Leningrad, pp 339–382
251. Lvova AS, Feodosyev NN (1964) Zh Fiz Khim 38: 28
252. Levitsky VA, Sorokina SL, Skolis YuYa, Kovba ML (1985) Neorg Mater 21: 1357
253. Berezhnoy AS, Belik VYa, Gavrish AM, Gulko NV (1968) Neorg Mater 4: 1605
254. Solov'eva AE, Gavrish AM, Zoz EI (1974) Neorg Mater 10: 469
255. Korsakov IE (1993) PhD Thesis, Moscow State University, Moscow

256. Gorelov VP (1992) In: Ionic and electronic transport in solid-state systems (in Russian). Ural Dept of RAS, Sverdlovsk, pp 36–42
257. Arestova NV, Gorelov VP (1994) Elektrokhimiya 30: 988
258. Gorelov VP, Sharova NV, Sokolova YuV (1997) Elektrokhimiya 33: 1455
259. Gorelov VP, Arestova NV, Kurumchin EKh, Vdovin GK (1995) Neorg Mater 31: 370
260. Lyubkina IYa, Kononyuk IF (1985) Vestn Belorus Univ Ser 2 (1): 11
261. Prisedskii VV, Tretyakov YuD (1982) Neorg Mater 18: 1926
262. Gorelov VP, Balakireva VB (1997) Elektrokhimiya 33: 1450
263. Kononyuk IF, Dedkova LN (1988) Neorg Mater 24: 1695
264. Bazuev GV, Shveikin GP (1975) Neorg Mater 11: 2195
265. Bazuev GV, Shveikin GP (1975) Fizika Tverd Tela 17: 3453
266. Bazuev GV, Shveikin GP (1978) Neorg Mater 14: 267
267. Perfilyev MV, Demin AK, Kuzin BL, Lipilin AS (1988) High-temperature electrolysis of gases (in Russian). Nauka, Moscow
268. Chebotin VN, Perfilyev MV (1978) Electrochemistry of solid electrolytes (in Russian). Khimiya, Moscow
269. Murygin IV (1991) Electrode processes in solid electrolytes (in Russian). Nauka, Moscow
270. Kuzin BL, Vlasov AN (1984) Elektrokhimiya 20: 1636
271. Kuzin BL, Komarov MA (1990) Elektrokhimiya 26: 1443
272. Naumovich EN, Kharton VV, Vecher AA (1998) Ceramic materials for high temperature electrochemical devices. In: Sviridov VV (ed) Chemical problems of developing novel materials and technologies (in Russian). Belarus State University, Minsk, pp 431–450
273. Ivanova NP, Kozhukh AV, Sonin VI, Zharsky IM, Pakhomov VP (1988) Elektrokhimiya 24: 234
274. Shuk PP, Tichonova LA, Guth U (1994) Solid State Ionics 68: 177
275. Kharton VV, Naumovich EN, Zhuk PP, Tonoyan AA, Vecher AA (1992) Vesti Akad Nauk Belarusi Ser Khim (2): 35
276. Kharton VV, Zhuk PP, Naumovich EN, Zinkevich MV, Vecher AA (1991) USSR Patent 1763421
277. Kharton VV, Zhuk PP, Naumovich EN, Vecher AA, Tonoyan AA (1991) USSR Patent 1794931
278. Kovalevsky AV, Kharton VV, Naumovich EN (1996) Inorg Mater 32: 1230
279. Kharton VV, Naumovich EN, Vecher AA (1999) J Solid State Electrochem 3: 61
280. Vdovin GK, Kuzin BL, Kurumchin EKh (1991) Poverkhn Fiz Khim Mekh (10): 30
281. Vdovin GK, Kurumchin EKh (1993) Elektrokhimiya 29: 1366
282. Kuzin BL, Komarov MA, Nikolaeva ER (1992) Elektrokhimiya 28: 1490
283. Gorelov VP, Kurumchin EKh (1986) Kinet Katal 27: 1346
284. Kurumchin EKh (1990) Studying the boundary of oxygen-solid electrolyte based on ZrO_2, Bi_2O_3 or CeO_2 by oxygen isotopic exchange method. In: Perfilyev MV (ed) Electrode reaction in solid electrolytes (in Russian). Academy of Sciences of USSR, Ural Dept, Sverdlovsk, pp 63–79
285. Kurumchin EKh, Vdovin GK, Gorelov GP, Zhuk PP, Naumovich EN (1993) Oxygen isotropic exchange of bismuth oxide-based electrolytes with gaseous oxygen. In: Perfilyev MV (ed) Ionics of solid state (in Russian). Nauka, Ekaterinburg, pp 39–45